Journal of Hydrology 679 (2026) 136159

Contents lists available at ScienceDirect

Journal of Hydrology

journal homepage: www.elsevier.com/locate/jhydrol

Hydrogeochemical assessment and vulnerability analysis of mountain springs in a karstic water system in northeastern Italy

Mauro Masiol [a,*], Maria Battistel [a], Lucio D'Alberto [b], Marianna D'Amico [a], Giovanni Mario [a], Raffaele Marciano [c], Giuliano Dreossi [a], Alessandro Pozzobon [b], Barbara Stenni [a]

[a] Dip. Scienze Ambientali, Informatica e Statistica, Università Ca' Foscari Venezia, IT-30172 Mestre-Venezia, Italy
[b] Servizio Osservatorio Acque Interne, Agenzia Regionale per la Prevenzione e Protezione Ambientale del Veneto (ARPAV), IT- 35121 Padova, Italy
[c] Piave Servizi S.p.A., IT-31013, Codogné TV, Italy

ARTICLE INFO

This manuscript was handled by Dr. D Han, Editor-in-Chief

Keywords:
Aquifer recharge
Protection zones
Spring water geochemistry
Stable water isotopes
Mountain spring hydrogeology
Vulnerability assessment

ABSTRACT

Mountain springs are essential freshwater resources for both communities and ecosystems, but they are increasingly threatened by climate variability and human pressure. This study investigates the vulnerability and recharge dynamics of two springs (LAR and CAN) in the Cansiglio Massif karst system (NE Italy). The novelty of this work lies in applying an integrated hydrogeological, hydrogeochemical, isotopic, and vulnerability-based framework to two springs in the foothills of a main karst system, showing how multiple complementary techniques can support the definition of recharge areas and protection zones even for small sources that remain essential for local water-supply management. Monitoring (September 2018 to September 2021) shows that recharge likely originates from the Mt. Pizzoc area and follows structurally and topographically controlled pathways toward the springs. Results reveal a dual recharge regime: rapid infiltration through fractured and karstified carbonates and coarse slope deposits, and slower, laterally redistributed flow where marly-silty-clayey layers hinder vertical percolation. A simplified water budget constrained the minimum and net recharge areas, while isotope-elevation relationships estimated mean recharge elevations of about 732–879 m a.s.l. for LAR and 617–767 m a.s.l. for CAN. Hydrological patterns and vulnerability indicators show that CAN responds much faster and is far more vulnerable (VESPA V = 14–38.7; MDHT 1–4 days) than LAR (VESPA V = 0.36–0.77; MDHT 9–22 days). By combining multiple approaches, this integrated framework offers practical support for identifying protection priorities, especially in shallow and highly responsive mountain spring catchments.

1. Introduction

Mountain aquifers are among the most valuable water resources in Northern Italy, supporting ecological balance and the well-being and resilience of local communities. Owing to their generally high water quality, mountain springs provide a primary freshwater source (Viviroli et al., 2007; Parise and Sammarco, 2015; Obolewski et al., 2016; Liu et al., 2018; Somers and McKenzie, 2020) and an important resource for downstream users. They sustain multiple sectors, including agriculture and livestock farming, hydropower production, artificial snowmaking, and industrial activities (Lucianetti et al., 2020). Despite their importance, mountain catchments are sensitive ecosystems that are vulnerable to anthropogenic pressures (e.g., deforestation, land-use changes, soil sealing, contamination). Because many springs are fed by shallow groundwater flow circuits, they are particularly susceptible to contamination (Viviroli et al., 2007; Amanzio et al., 2015; Parise et al., 2015; Obolewski et al., 2016; Liu et al., 2018; Somers and McKenzie, 2020; Stevanović, 2019; Lo Russo et al., 2021; Lorenzi et al., 2024; Çallı et al., 2025). Their vulnerability is further increased by climate-change impacts, including shifts in precipitation patterns (Wu et al., 2020; Notarnicola, 2020), which can reduce recharge and affect spring discharge (Cisneros et al., 2014).

In recent decades, hydrological challenges have intensified in the mountainous regions of Italy (Alps and Apennines). Studies report spring drying, reduced discharge during dry periods, and the transition of previously perennial springs into seasonal ones (e.g., Fiorillo and Guadagno, 2012; Fiorillo et al., 2015a; Fiorillo et al., 2015b; Fiorillo and Pagnozzi, 2015; Forestieri et al., 2018; Padulano et al., 2019; Fiorillo et al., 2021; Gizzi et al., 2022; Azimi et al., 2023). Climate models indicate that the Mediterranean region will experience increasingly

* Corresponding author.
E-mail address: mauro.masiol@unive.it (M. Masiol).

https://doi.org/10.1016/j.jhydrol.2026.136159
Received 14 April 2026; Received in revised form 15 July 2026; Accepted 31 July 2026
Available online 6 August 2026

intense and frequent droughts (Padulano et al., 2021), potentially affecting both the availability and quality of mountain spring water. Accurately quantifying and characterizing mountain groundwater is therefore essential for current and future management and for assessing climate-change impacts on water resources (Leone et al., 2020; Çelik et al., 2024). The combined use of vulnerability indices and analytical models is increasingly applied to support decision-making and spring-protection frameworks (Foster et al., 2013; Javadi et al., 2019). A key initial step is to investigate geochemical characteristics, understand hydrological regimes, and delineate protection areas. Pochon et al. (2008) proposed methods for defining protected areas based on spring vulnerability, while Civita (2008) introduced the MDHT (annual maximum discharge half-time) derived from spring hydrographs. Galleani et al. (2011) developed the VESPA (Vulnerability Estimator for Spring Protection Areas) index using discharge, electrical conductivity, and temperature measured at the spring site; VESPA has since been applied to assess vulnerability and delineate protection zones for mountain springs in Northern Italy (Galleani et al., 2011; Banzato et al., 2017; Torresan et al., 2020).

The mountainous region of Northeastern Italy (Fig. 1a), including the

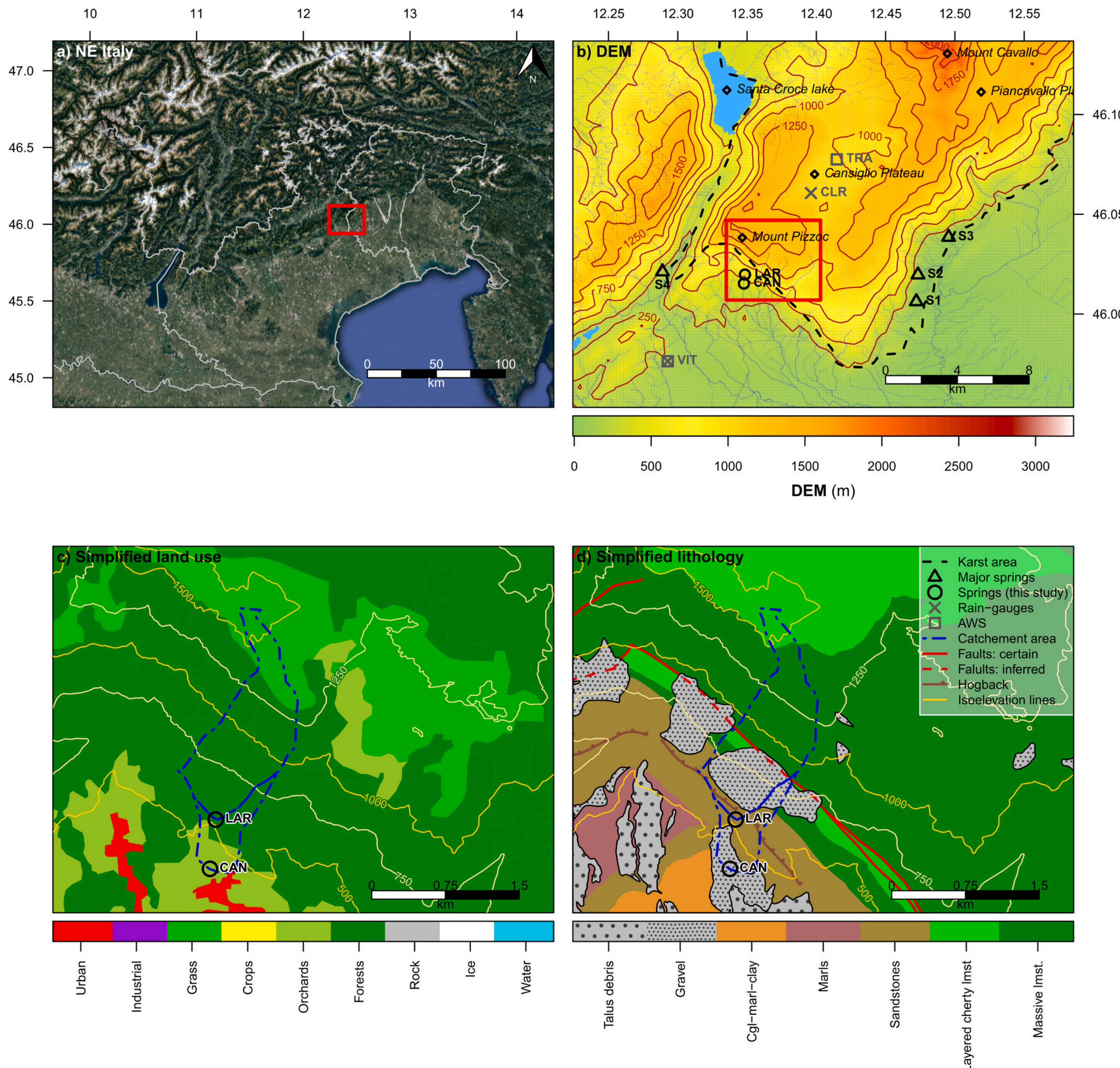

Fig. 1. Maps of the study area: a) geographical framework across NE Italy; b) zoom to the southern corner of the Cansiglio plateau (Cansiglio–Cavallo massif) showing the terrain relief from digital elevation model (EEA, 2016), the extension of the Karst area (Filippini et al., 2018), the location of the main springs (S1 = Molinetto; S2 = Santissima; S3 = Gorgazzo; S4 = Meschio), the location of the springs investigated in this study, rain-gauge stations and automatic weather stations (AWSs); c) further zoom on the study area showing simplified land-cover classes generated using European Union's Copernicus Land Monitoring Service information CORINE Land Cover 2018 (vector) (EEA, 2020, see SI section 1 for details); d) simplification of the Mesozoic-Tertiary succession of the study area from the geological map of the province of Treviso, sections 064130 Fregona-Mezzavilla and 064140 Coltura (modified from Bondesan et al., 2013). For security and regulatory reasons related to drinking-water supply infrastructure, the map reports generalized hydrogeological features and inferred protection areas rather than exact georeferenced locations of aqueduct facilities or intake structures.

Prealps, belongs to the Alpine system and, more specifically, to the Southern Alps, characterized by complex tectonics and diverse geological formations (e.g., Caputo et al., 2010). The interplay of lithologies, structure, topography, and climate has produced widespread karst features (Cucchi and Finocchiaro, 2017; Xanke et al., 2024), e.g. on Mt. Canin and in the Cansiglio-Cavallo Massif located in the Forealps (Carnic Prealps). This major karst area hosts a substantial aquifer and numerous springs that sustain local communities (Vincenzi et al., 2011; Filippini et al., 2018). Despite abundant rainfall in the region (Toreti et al., 2009), surface waters are scarce because sinkholes and swallow holes promote rapid infiltration, concentrating discharge along massif slopes. While the main spring recharge areas have been investigated (e.g., Filippini et al., 2018), many smaller springs on the southwestern slope remain less understood, motivating hydrogeological characterization to support sustainable management and long-term protection.

Previous investigations in the Cansiglio-Cavallo Massif have substantially improved the understanding of the main karst aquifer, especially investigating the three basal springs feeding the Livenza River, through tracer tests, hydrological monitoring, hydrochemistry, and isotopic analyses. These studies demonstrated the role of the Cansiglio Plateau as a major recharge area and highlighted the structural control exerted by faults and lithological contrasts on groundwater flow. However, the connection between the main recharge area and the major springs is not yet fully understood. Under this view, karst aquifers are intrinsically difficult to characterize because of their high heterogeneity and anisotropy. Rapid infiltration and preferential flow through complex conduit networks often decouple surface and groundwater catchments, making recharge-discharge relationships highly uncertain and difficult to quantify (Fiorillo et al., 2022). Also, the complexity of epikarst (Milanović, 2025) may affect water infiltration. In addition, most studies on mountain spring systems focus on large and regionally important springs, whereas minor springs supplying small communities or even a limited number of households are much less frequently investigated. From a regulatory and water-management perspective, however, these small sources cannot be considered marginal (Parise and Sammarco, 2015; Parise et al., 2015): water utilities must guarantee safe drinking water independently of the number of users supplied, while also improving aqueduct infrastructure, optimizing management, and assessing whether the source is adequately protected from potential pollutants.

The present study investigates the hydrogeological and geochemical functioning of two small springs on the southern slopes of the Cansiglio-Cavallo Massif, overlooking the Po Plain (Fig. 1a–d), with three main objectives: (i) delineate the potential groundwater recharge areas feeding the springs, (ii) assess their intrinsic vulnerability to contamination, and (iii) define spring safeguard (protection) areas to support management of these resources. The springs are representative of many small mountain supplies that require monitoring and protection because they contribute to local distribution networks. However, robust approaches for vulnerability assessment at this scale remain debated, as does the hydrogeological setting of such springs, particularly whether they are hydraulically connected to the broader Cansiglio karst system or instead drain small, independent basins.

To address these issues, hydrogeological (discharge measured with high temporal resolution) and hydrogeochemical variables (field physico-chemical parameters and major-ion concentrations with pseudo-monthly resolution) were monitored together with the oxygen and hydrogen isotopic composition ($\delta^{18}O$ and $\delta^{2}H$) of both spring water and local precipitation. Finally, the VESPA index was applied to quantify vulnerability and delineate safeguard zones, integrating hydrological, chemical, and isotopic evidence to interpret the processes controlling spring-water quality and to inform effective spring-protection measures.

The original contribution of this study lies in the integrated assessment of two previously uncharacterized minor springs with discharges ranging from a few to hundreds of L s^{-1}, developed through a joint perspective involving researchers, environmental technicians, and the Water Utility. Unlike previous studies focused mainly on the major basal karst springs of the Cansiglio system, this work addresses small mountain springs located along the slope, where recharge may involve both debris-covered sectors and fractured or karstified bedrock. By combining high-frequency discharge, temperature, and electrical-conductivity monitoring with major-ion chemistry, stable water isotopes, simplified water-budget estimates, and VESPA/MDHT vulnerability metrics, the study constrains effective recharge elevations and areas, identifies contrasting flow regimes, and evaluates how large the protection area should be to safeguard the aquifer. In this way, the manuscript advances previous work by linking spring-outlet vulnerability indicators with recharge-area reconstruction and by providing a practical framework for protecting small but operationally important drinking-water sources in complex mountain hydrogeological settings.

2. Materials and methods

2.1. Study area

The Cansiglio-Cavallo Massif is composed predominantly of sedimentary carbonate rocks ranging from the Triassic to the Late Cretaceous, overlain by terrigenous units up to Miocene and related to the Alpine orogeny (Cancian et al., 1985). The area encompasses the Prealps sector and the western margin of the Friulian Platform, where multiple depositional environments are represented and anticline structures commonly expose carbonate rocks in their cores. The region initially developed as a shallow-marine platform bordered to the west by a steep escarpment that connected the platform to the deep-sea Belluno Basin. From the Jurassic to the end of the Late Cretaceous, an extensive orogenic reef system formed along this margin. Subsequent platform subsidence during the latest Cretaceous led to an eastward retreat of the escarpment and a transition to deep-marine conditions, promoting the accumulation of terrigenous deposits, including Scaglia Rossa limestone (Upper Cretaceous–Eocene). In the Late Miocene, the Neo-Alpine phase of the Alpine orogeny uplifted and exposed the area, shaping the present-day geomorphology and hydrological framework.

The area is characterized by two large basins of karstic origin, the Piancavallo and the Pian del Cansiglio (Fig. 1b). This latter is a limestone and relatively flat, polje-like depression at about 1000 m a.s.l., bounded by higher ridges generally reaching 1300–1500 m a.s.l. along its western to southeastern margins. These include Mt. Pizzoc (1565 m a.s.l.), located about 2 km north of LAR, while the higher Mt. Cavallo massif (2251 m a.s.l.) is located to the northeast. The Cansiglio-Cavallo area hosts one of the most important karst aquifers in northern Italy (Cucchi and Finocchiaro, 2017; Filippini et al., 2018) but its hydrogeology is still poorly known (Vincenzi et al., 2011); the watershed covers an area of ~53 km^2. Despite abundant precipitation, surface drainage on the massif is almost absent because of the presence of well-developed epigean and hypogean karst landforms, including numerous dolines, sinkholes, shafts, and mainly vertical karst cavities (Castiglioni, 1964; Grillo, 2007; Vincenzi et al., 2011) that rapidly convey meteoric recharge underground, allowing the system to function as an endorheic basin with an articulated network of underground canalization, the hypogean extent of which is relatively unknown. More than 250 known caves have been discovered in the area, mostly with a predominantly vertical development (deep shafts), few of which are deeper than 100 m, such as Bus de la Genziana (depth of 587 m and a development of 8 km, (Cancian and Ghetti, 1989; Riva, 2000), Bus de la Lum (185 m), and Abisso del Col della Rizza (800 m below topographic surface) (Grillo, 2007; Grillo et al., 2011; Vincenzi et al., 2011). Although many caves have been explored, major underground rivers have not been directly identified, so the internal drainage pathways remain only partly known (Grillo, 2007; Vincenzi et al., 2011).

Surface water is mainly found at the foothills of the massif: to the Northwest, in the Lapisina Valley, where some lakes (Morto, Restello) and the Meschio Creek are located (Fig. 1b), the latter being largely fed and regulated by hydropower plants; at the southern and southeastern base of the massif, where the Livenza River originates; and to the West, where small springs emerging along the hilly ridges feed minor creeks. The Livenza is fed by three major springs (Molinetto, Santissima and Gorgazzo, Fig. 1b) with a mean discharge of about 8–11 $m^3\ s^{-1}$ (Vincenzi et al., 2011; Filippini et al., 2018) at elevations of 20–50 m above sea level (m a.s.l.) (Meneghel et al. 1986). These springs are aligned along a ~5 km resurgence front controlled by the Caneva–Maniago fault, where Mesozoic limestones are juxtaposed against less permeable Tertiary molasse (Filippini et al., 2018).

Numerous studies have been completed in the area. Geodetic measurements (Grillo et al., 2011; Grillo et al., 2018; Devoti et al., 2015) generally showed that meteoric recharge in the Cansiglio-Cavallo massif is routed through the karst system towards the southwestern Friulian Plain. More recently, Pintori et al. (2021) indicated that the Cansiglio-Cavallo karst system is part of a highly permeable, fault-controlled aquifer network in which groundwater-storage changes can rapidly focus pressure into fractures, producing transient horizontal deformation and stress perturbations that may influence local seismicity. Hydrogeological surveys of precipitation, cave waters and the main Livenza springs by Grillo (2007) showed a shallow karst network of directly draining conduits and channels; in Bus de la Genziana, isotopic evidence further revealed a complex hydrological circuit in which water from higher elevations feeds the deeper cave levels and mixes with the main flow. Water monitoring in Bus de la Genziana cave (Grillo and Braitenberg, 2016) shows that rainfall rapidly triggers cave flooding within hours, confirming highly conductive underground circuits, but the cave water represents only a small fraction of spring discharge and comes from multiple directions, indicating a direct, multi-drainage karst system. Vincenzi et al. (2011) performed a first fluorescent tracer test and detected a connection between an 800 m-deep cave (Abisso Col de la Rizza) in the Cansiglio plateau with two major springs (Molinetto and Santissima) while no connection was demonstrated for another cave (Bus de la Genziana) (Fig. 1b). A work by Filippini et al. (2018), supported by isotopic monitoring of springs and precipitation, further constrains the origin of the three major springs draining the karst aquifer and feeding the Livenza River. These springs have distinct recharge areas; they behave as partly independent drainage systems during low flow, while high-flow conditions produce more similar geochemical signatures across all springs.

While the major karst springs feeding the Livenza River have been extensively studied, this work focuses on two minor springs located on the southwestern slope of the Cansiglio–Cavallo massif. Laron (LAR) spring emerges at 522 m a.s.l. from fractures in a bench of slightly marly bioclastic limestone (Monte Baldo Formation), whereas Canchero (CAN) spring issues diffusely from carbonate slope debris at 397 m a.s.l. Both springs, together with others not considered in this study, emerge along the slope of the massif at elevations significantly higher than the main basal springs (Santissima, Molinetto, and Gorgazzo). Springs on this southwestern slope have not previously been investigated; consequently, their possible hydraulic connection to the main karst system of the Cansiglio Plateau remains unknown.

The area is characterized by a humid temperate climate, influenced by both the Adriatic Sea and the Alpine barrier. Precipitation is moderately distributed throughout the year, with typical minima in winter and summer and maxima in late spring (May) and late autumn (November). Orographic effects enhance rainfall in mountainous and pre-alpine areas, while lower precipitation totals occur over the plains. Mean annual precipitation for 2000–2024 was ~2160 mm yr^{-1} at the plateau (range 1175–3217 mm yr^{-1}) and ~1470 mm yr^{-1} at the bottom of the massif toward the Po Plain edge (range 738–2312 mm yr^{-1}). Mean temperatures show warm summers and cool winters, with increasing continentality toward inland and elevated areas.

2.2. Flow data collection

Continuous hydrological data were collected from September 2018 to September 2021 in both springs using OTT HydroMet Orpheus mini (Germany) multi-parameter CTDs (Conductivity, Temperature, Depth) sensors with integrated data loggers. These devices collected data at 12-min intervals: water temperature (°C), water level (expressed as bar in LAR and in m at CAN) with a vented pressure cell recording hydrostatic pressure of the water column and automatically compensating for atmospheric pressure, and specific electrical conductivity (EC, expressed as μS cm^{-1} at 20 °C) with a 4-electrode graphite cell.

At LAR, the probe was installed inside a perforated tube placed in a natural pool formed by the spring, approximately 2 m upstream of the concrete spillway leading to sedimentation and loading tanks (Fig. S1). The pool is about 70 cm deep, and the probe was positioned a few centimeters above the bottom. A dry period at the LAR spring lacked manual measurements, so zero-discharge pressure ($P_0 \approx 0.0697$ bar) was indirectly estimated from pressure-water head relations. P_0 was then subtracted from all pressure data to obtain corrected values (P^*) used to define the discharge curve. Details of this conversion are provided in SI Section S2.

At CAN, the probe was installed in the loading tank within a perforated support tube, positioned a few centimeters above the bottom and approximately 40 cm far from the supply pipe (Fig. S2). During the monitoring period at CAN, the probe recorded abrupt drops in water level, likely due to hydraulic operations carried out by the managing authority for regular maintenance and/or to compensate for insufficient withdrawals from the LAR spring. These operations involved increasing the opening of the supply pipe valves beyond normal conditions, resulting in enhanced water extraction and a consequent decrease in the tank water level. As these measurements were affected by operational disturbances, the corresponding water-level data were excluded from the analysis.

At LAR, the relationship between sensor-recorded water level and discharge was established using two methods: (i) direct discharge measurements at medium to high flows using either a Seba Hydrometrie GmbH & Co. (Germany) M1 propeller current meter or an OTT (Germany) MFpro electromagnetic flow meter over the concrete weir; or (ii) the volumetric method at low flows by measuring the time required to fill a 10 L container (average of 3 measurements). At CAN, where the spring intake configuration prevented total direct discharge measurements across the entire flow range, total discharge was calculated as the sum of the flow measured by the flow meter installed on the intake pipeline and the overflow across the thick concrete weir (measured using the same setup described for LAR).

2.3. Spring and precipitation water sampling

Spring water samples for chemical, physical, and isotopic analyses were collected monthly at LAR and CAN between July 2019 and September 2021. Two aliquots were collected: one for chemical analyses and one for isotopic analyses. Meteoric water samples were collected monthly using rain gauges designed to prevent evaporation, following IAEA/GNIP recommendations (IAEA, 2014). Rain gauges were installed at two different elevations: Vittorio Veneto (VIT; 172 m a.s.l.) and Pian Cansiglio Le Rotte (CLR; 1065 m a.s.l.) (Fig. 1). All collected samples were stored refrigerated in 50 mL HDPE bottles with airtight caps until analysis to prevent degradation and fractionation.

2.4. Water isotope and chemical analyses

Hydrochemical and isotopic investigations provide useful information for groundwater protection and delineating recharge areas of karst aquifers (e.g., Petitta et al., 2022; Lorenzi et al., 2024; Petitta et al., 2026). Spring water was analysed for major physicochemical parameters and dissolved constituents, including alkalinity (expressed as mg

L^{-1} $CaCO_3$), electrical conductivity (μS cm^{-1} at 20 °C), hardness (French degrees, where 1 °fH corresponds to 10 mg L^{-1} of calcium carbonate), pH, and the concentrations (mg L^{-1}) of bicarbonate (HCO_3^-), fluoride (F^-), chloride (Cl^-), bromide (Br^-), nitrate (NO_3^-), nitrite (NO_2^-), phosphate (PO_4^{3-}), sulphate (SO_4^{2-}), sodium (Na^+), magnesium (Mg^{2+}), potassium (K^+), calcium (Ca^{2+}), and silica (SiO_2), were analysed at VERITAS certified laboratories following standard methods (details reported in Table S1). Spring and precipitation waters were analysed for the isotopic composition ($\delta^{18}O$, δ^2H) by primarily adopting the well-established CO_2–H_2/water equilibration method adapted from Epstein and Mayeda (1953) with an automatic equilibration device (Finnigan MAT HDO 1086, United States) coupled to an isotope ratio mass spectrometers (IRMS; Thermo-Fisher Delta Plus Advantage, United States). Approximately 5% of samples were analysed by cavity ring-down spectroscopy (CRDS) using a PICARRO (United States) L2130-*i* analyzer equipped with a V1102-*i* vaporizer and an HTC PAL autosampler (CTC Analytics, Switzerland). To minimize between-sample memory effects in CRDS measurements (Penna et al., 2012), each sample was injected eight times and results were filtered by excluding values outside the mean ± one standard deviation. Analytical precision was $\leq \pm 0.05$‰ for $\delta^{18}O$ and $\leq \pm 0.7$‰ for δ^2H using IRMS, and $\leq \pm 0.10$‰ for $\delta^{18}O$ and $\leq \pm 0.5$‰ for δ^2H using CRDS. Consistency between the IRMS and CRDS methods was routinely verified through periodic cross-checks of results and regular monitoring of instrument performance. Routine inter-laboratory tests were conducted to ensure interoperability and to produce a consistent dataset (Masiol et al., 2021). Isotopic results are reported in standard delta (δ) notation in per mil (‰) relative to the VSMOW international standard.

Deuterium excess (d-excess = $\delta^2H - 8 \cdot \delta^{18}O$; Dansgaard, 1964) complements δ values by providing information on evaporation conditions at precipitation sources, mainly relative humidity, sea surface temperature, and partly wind speed (Kendall et al., 2014; Pfahl and Sodemann, 2014). Positive d-excess values result from kinetic fractionation during evaporation, when isotopic equilibrium between liquid and vapor is not fully achieved.

2.5. Weather data

Hourly meteorological data, including precipitation (mm), air temperature at 2 m above ground level (°C), maximum relative humidity (%), and minimum relative humidity (%), representative of the rain-gauge sampling sites, were obtained from two automatic weather stations (AWSs) managed by ARPAV: Vittorio Veneto (VIT; 123 m a.s.l.) and Cansiglio Tramedere (TRA; 1022 m a.s.l.). TRA was used as the reference station for the climate of CLR. Both TRA and CLR are located on the Cansiglio plateau, at a similar elevation and about 2.3 km apart.

2.6. VESPA index

To preserve water quality, it is necessary to assess the vulnerability level of an aquifer and the springs it feeds (Banzato et al., 2017). In Europe, several methods have been proposed and applied to assess aquifer vulnerability, including DRASTIC (Aller et al., 1987), SINTACS (Civita and De Maio, 1997), and GOD (Foster, 1987). Their application requires hydrostratigraphic information that is often unavailable in mountainous areas (Banzato et al., 2017). These methods require numerous data, such as water-table depth, effective infiltration, characteristics of the unsaturated zone, soil type, aquifer lithology, aquifer hydraulic conductivity, and surface slope. Other methods have been proposed based exclusively on discharge monitoring data and a few physico-chemical parameters measured at springs. Among these, the MDHT (Civita, 2008) and the VESPA index (Galleani et al., 2011) can be applied to springs with continuous monitoring of water level, temperature, and conductivity.

The VESPA index is based on the concurrent analysis of spring discharge, temperature, and specific electrical conductivity time series derived from continuous monitoring. Its application requires data collected over at least one complete hydrological year, with an hourly or bi-hourly sampling frequency, to adequately capture both baseline conditions and rapid system responses. Such high-resolution monitoring is essential to properly represent short-lived but hydrologically significant flood events, whose effects might otherwise be underestimated or missed, thereby improving the reliability and reducing uncertainties in vulnerability assessment (Galleani et al., 2011). The index is defined as multiplying 3 values: c(ρ), the correlation factor calculated between discharge and electrical conductivity over a one-year period; β, temperature variability factor; and γ, the discharge factor. Beyond defining spring vulnerability (low to very high), the VESPA index also identifies system behaviour (dominant conduits, piston flow, or dispersive circulation) and drainage effectiveness based on the correlation coefficient ρ (Galleani et al., 2011). Details of the method are provided in SI Section S3.

2.7. Definition of the recharge area and safeguard zones

Following vulnerability assessment, additional hydrogeological investigations are often required to delineate spring protection areas, especially when index-based or simplified approaches are used. Emphasis should be placed on the homogeneity of the aquifer and the identification of preferential infiltration zones in the catchment area. Vulnerability mapping methods are suitable for outlining protection areas in heterogeneous environments supplying highly vulnerable springs, particularly when preferential infiltration zones are identified in the catchment area. The delineation of specific spring protection areas may vary according to the local regulatory framework. Italian legislation requires regions (e.g. Veneto Region) to identify safeguard areas, which are divided into (i) absolute protection zones and (ii) respect zones, further divided into restricted and enlarged subzones, as well as additional protection zones within water basins and groundwater recharge areas. The identification and formal approval of protection areas involve both technical and administrative steps, including hydrogeological investigations and consultation with relevant stakeholders (water utility companies, "*Consigli di Bacino*", municipalities, Provinces, local health and local environmental authorities). Following approval by the regional council, municipalities are in charge to enforce the restrictions.

The absolute protection zone encompasses the area immediately surrounding water intakes or abstractions and must be strictly safeguarded, with land use limited exclusively to intake works and essential service infrastructure, in order to prevent any direct contamination risk. Surrounding this core area, the respect (buffer) zone extends over a wider portion of the territory and is subject to land-use restrictions specifically designed to preserve both the quality and the quantity of the water resource. Within the respect zone, all activities that could introduce pollutants or alter recharge processes (e.g., the discharge of sludge or treated wastewater, storage or use of fertilizers and pesticides, construction of cemeteries, waste management operations, storage of hazardous substances, and livestock grazing or housing) are prohibited or restricted, thereby ensuring long-term protection of the captured water.

3. Results and discussion

3.1. Flow rates and discharge regimes

During the sampling campaign, the yearly precipitation was ~2600 mm y^{-1} at TRA (~21% higher than the 2000–2024 average) and ~1525 mm y^{-1} at VIT (+4%). The higher averaged (TRA + VIT) monthly precipitation was recorded in November 2019 (584 mm) and April 2019 (540 mm).

The reconstruction of flow rates (Q) was determined by regressing hourly-averaged CTD pressure data over the manual flow readings. Since the relationship between the dependent and independent variables is not known a priori, several curves were tested to find the optimal fit, including linear, polynomials, quadratic, exponential and spline). For LAR, pressure values ranged from 0.069 to 0.086 bar, with two modes at 0.074 and 0.078 bar. The 16 in-situ manual discharge measurements covered the full range of observed pressures, including both low and high values (Fig. S3a). This homogeneous distribution ensures that the regression is constrained by data across the entire pressure domain, resulting in a robust reconstruction that is representative of the full range of operating conditions. A 2nd order polynomial was chosen for better fit the data (3-fold cross-validated root mean squared error (cv-RMSE) = 2.4 L s^{-1}; R^2 = 0.98; Fig. S3b). The polynomial regression was further run for the assessment of the prediction uncertainty by also accounting for the uncertainties in the relative measurement in the dependent variable (in-situ flow measurements) and the uncertainty associated to the independent variable (CTD pressure), propagated through the local derivative of the fitted polynomial. Details are reported in Section S4.

For CAN, after discarding values below 0.42 m due to pressure drops recorded during service operations, water levels ranged from 0.42 to 0.69 m and exhibited a pseudo-lognormal distribution peaking at approximately 0.45 m (Fig. S5a). In-situ manual discharge measurements covered a water level range of ~0.40–0.60 m, i.e. overlapping with most (~96.5%) of the continuous records. However, no field measurements were collected at the highest water levels (~4.5% of total records), and thus at the highest discharges. Although this could represent a limitation for discharge reconstruction due to the lack of direct constraints at high levels, the relationship between manual and automatic data at high values shows a very strong linear relation (R^2 > 0.99), supporting the assumption of linear behaviour. Consequently, discharge reconstruction was improved using a piecewise regression, with a quadratic fit at low water levels and a linear fit at high water levels. The optimal breakpoint, determined by minimizing cross-validated RMSE and Mean Absolute Error (MAE), was set at 0.49 m. The final model is shown in Fig. S5b, and discharge values below the minimum manually measured flow (0.42 m) were set equal to that minimum. Prediction uncertainty was estimated similarly to LAR (water level as independent variable) but for predictions beyond the calibration range, an additional conservative uncertainty term increasing with the distance from the calibration domain was further included to account for the reduced reliability of extrapolation (Section S4 and Fig. S6).

An initial assessment of spring behaviour was carried out by comparing water temperature (T, expressed as °C) and electrical conductivity (EC, μS cm^{-1} at 20 °C) measured during the monitoring campaign with the corresponding hydrographs (Figs. 2–3(a–c)). Two data gaps were identified at LAR due to probe malfunctions: one between July and August 2019 and another lasting approximately 20 days in September 2021. Moreover, temperature and conductivity measurements collected during a dry period (12 days between October and November 2019) were excluded from the statistical analysis, as water stagnation may have affected data reliability. For CAN, six periods of missing discharge data were identified, resulting from abrupt water-

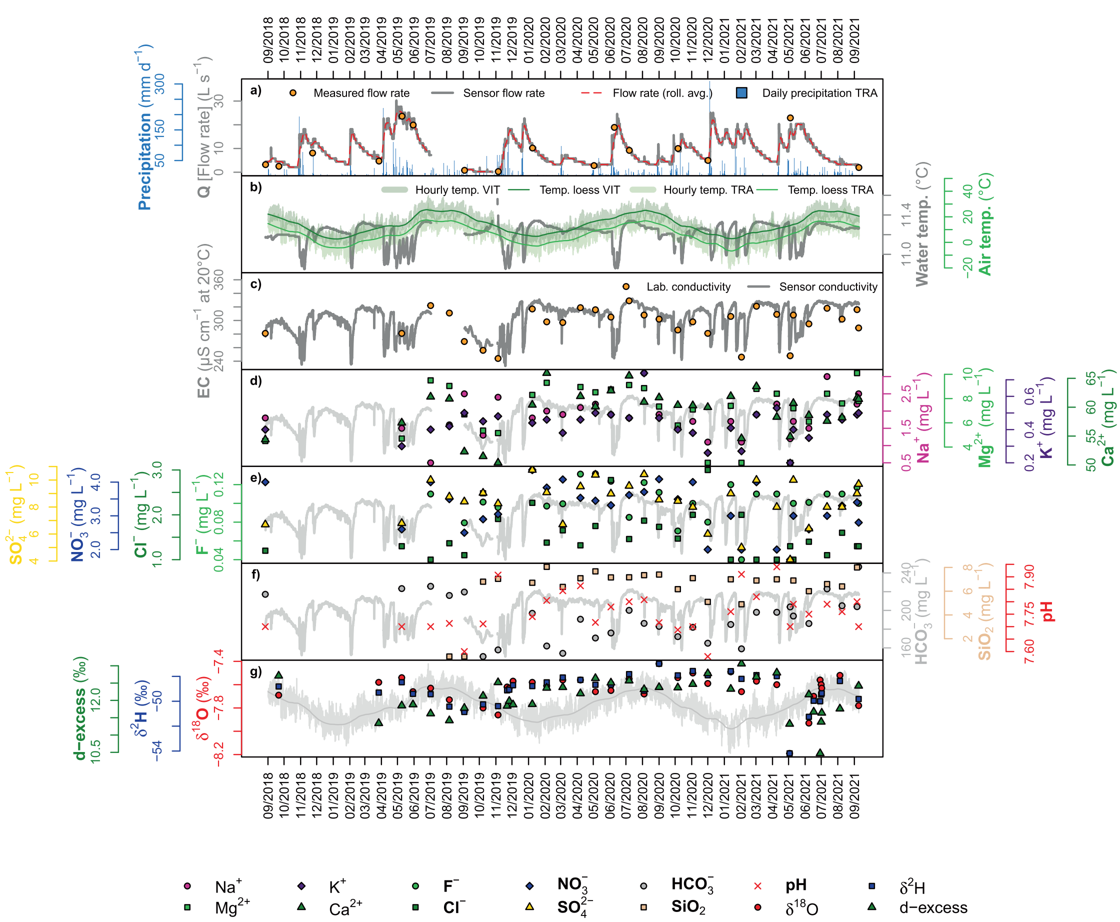

Fig. 2. Time series of hydrometeorological and hydrochemical variables collected at LAR. (a) Hourly-averaged spring discharge (Q, L s^{-1}) and daily cumulative precipitation (mm d^{-1}) recorded at the TRA weather station; the 7-day moving-average discharge is also shown. (b) Mean hourly spring-water temperature and air temperature at 2 m above ground level measured at the TRA (light green) and VIT (dark green) AWSs, with LOESS-smoothed trends superimposed. (c) Electrical conductivity (EC, μS cm^{-1} at 20 °C) measured continuously in situ (grey line) and on discrete samples analysed in the laboratory (yellow symbols). (d) Anion concentrations, (e) cation concentrations, and (f) pH together with carbonate and silica concentrations (symbols); panels (d–f) include the EC record in the background for reference. (g) Isotopic composition ($\delta^{18}O$, δ^2H and deuterium excess); the LOESS-smoothed air temperature at TRA is shown in the background. (For interpretation of the references to colour in this figure legend, the reader is referred to the web version of this article.)

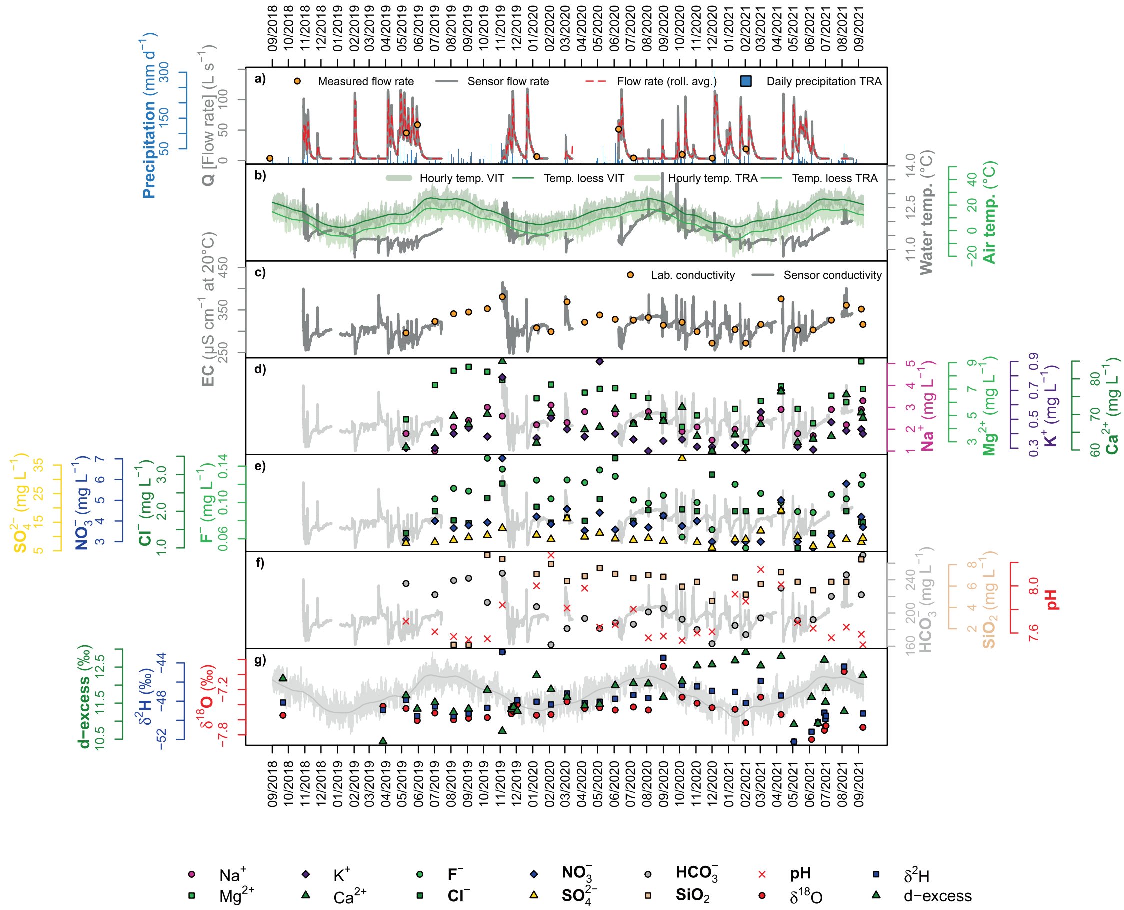

Fig. 3. Time series of hydrometeorological and hydrochemical variables collected at CAN. (a) Hourly-averaged spring discharge (Q, L s^{-1}) and daily cumulative precipitation (mm d^{-1}) recorded at the TRA weather station; the 7-day moving-average discharge is also shown. (b) Mean hourly spring-water temperature and air temperature at 2 m above ground level measured at the TRA (light green) and VIT (dark green) AWSs, with LOESS-smoothed trends superimposed. (c) Electrical conductivity (EC, μS cm^{-1} at 20 °C) measured continuously in situ (grey line) and on discrete samples analysed in the laboratory (yellow symbols). (d) Anion concentrations, (e) cation concentrations, and (f) pH together with carbonate and silica concentrations (symbols); panels (d–f) include the EC record in the background for reference. (g) Isotopic composition ($\delta^{18}O$, δ^2H and deuterium excess); the LOESS-smoothed air temperature at TRA is shown in the background. (For interpretation of the references to colour in this figure legend, the reader is referred to the web version of this article.)

level drops recorded after hydraulic operations conducted by the water supplier.

The statistical distribution of discharge, water temperature, and electrical conductivity is illustrated in the violin plots of Fig. S7. LAR exhibited a discharge of (average ± st.dev.) 9 ± 6.1 L s^{-1}, ranging from 0 L s^{-1} to a maximum of 30.2 L s^{-1} recorded on 24 April 2019 (corresponding to one of the rainiest months during the monitoring campaign); the assessed uncertainty varied from 0.4 L s^{-1} at zero discharge to 2.8 L s^{-1} (∼9%) at maximum recorded discharge. CAN showed higher discharge, with a value of (mean ± st.dev.) 17.7 ± 23.8 L s^{-1} and a peak of 118 L s^{-1} on 21 December 2019; the assessed uncertainty varied from 0.7 L s^{-1} (∼20%) at minimum discharge to 10.5 L s^{-1} (∼11%) at maximum recorded discharge. Both springs are considered as highly variable by calculating the Meinzer's variability percentage from discharge data (Meinzer, 1923) as $((Q_{max}-Q_{min})/Q_{mean})\cdot 100$ with values of 338 and 651, respectively. Water temperature at LAR remained relatively stable throughout the monitoring period, with an average of 11.2 °C and a narrow range between 10.8 °C and 11.6 °C. CAN exhibited greater temperature variability, with a 10.7–13.7 °C range and an average of 11.6 °C. A similar pattern was observed for EC: LAR showed limited variability (mean 303 μS cm^{-1}, range 233–332 μS cm^{-1}), whereas CAN exhibited wider fluctuations, ranging from 246 to 415 μS cm^{-1}, with a mean value of 307 μS cm^{-1}. The higher variability in water temperature observed at CAN is likely linked to the shallow nature of the aquifer, which is more sensitive to atmospheric temperature fluctuations. Under this view, as shown in Fig. 3b, spring water temperature at CAN appears to follow the seasonal trend of air temperature, with an estimated time lag of approximately two months.

Increases in discharge at the LAR spring are often associated with decreases in both temperature and EC, indicating a rapid contribution of newly infiltrated water (Fig. 2a–c). This recharge water, having had limited residence time within the aquifer, is colder and less mineralized, effectively replacing resident groundwater. In contrast, discharge peaks at CAN are typically associated with an initial increase in temperature and EC, followed by a subsequent decrease (Fig. 3a–c). This pattern is characteristic of a piston-flow mechanism, commonly observed in interconnected karst systems or debris aquifers, where recharge-induced pressure mobilizes more mineralized resident water before newly infiltrated water reaches the outlet. However, CAN cannot be classified as a typical karst spring, as it emerges from superficial debris deposits on a slope. The post-precipitation increase in temperature and EC may therefore also reflect the rapid drainage of pore water stored within the debris. In this setting, the large water–rock contact surface enhances dissolution and mineralization processes, causing the water trapped between grains to become more mineralized before being displaced and flushed out by infiltrating water. Furthermore, water temperature at CAN follows a seasonal trend similar to air temperature, with an estimated lag of approximately two months, suggesting a shallow and rapidly responding recharge system.

Hydrograph analysis provides initial insight into the characteristics of the two springs (Fiorillo, 2014), as spring responses to recharge are controlled by recharge area size, rainfall intensity, and aquifer storage and transmissivity. Both LAR and CAN show pronounced discharge peaks following major precipitation events (Figs. 2–3(a)) but differ markedly in their recession behaviour. LAR displays a gentler recession, indicating a deeper aquifer system with greater storage and longer residence times. In contrast, CAN exhibits a steep recession, reflecting rapid drainage of a shallow system. This contrast is particularly evident in January–February 2021 (Fig. S8): CAN shows a clear piston-flow response during the rising limb, while LAR is dominated by replacement flow, with decreases in temperature and conductivity at peak discharge. These patterns suggest a short, shallow flow path for CAN, consistent with its higher temperature variability and mean temperature, and a deeper, more buffered system for LAR, as also indicated by its very low temperature variability (<1 °C).

Similar conclusions can be drawn from the analysis of the temporal relationship between precipitation and spring discharge using cross-correlation analysis (CCF). Precipitation was evaluated at an hourly scale using AWS data for the period in which continuous hydrological records were available from the CTD sensors. The results show a moderate correlation ($r \approx 0.6$) between precipitation measured at the foothill station (VIT) and on the mountain plateau (TRA) at lag = 0, indicating that rainfall is broadly synchronous across the study area (Fig. S9). Cross-correlation between hourly precipitation at TRA and spring discharge highlights distinct response times for the two springs (Fig. S10). LAR shows a broad plateau of low positive correlations ($r \geq 0.14$), with a maximum at lag −87 h ($r = 0.16$), suggesting a delayed and distributed response, with peak discharge occurring approximately 24 h to 10 days after rainfall. In contrast, CAN exhibits a sharp maximum correlation ($r \approx 0.4$) at lag −24 h, indicating a much faster hydrological response.

3.2. Chemical composition

The first water sample was collected at the start of the monitoring period, followed by monthly sampling from May 2019 to September 2021. Figs. 2 and 3(d–f) summarize the main hydrogeochemical variables, while Fig. S7 illustrates their statistical distributions and Fig. S11 presents the corresponding Schoeller diagrams. Overall, LAR shows slightly higher Mg^{2+} concentrations than CAN, whereas Ca^{2+} is lower (Figs. 2–3(d)). Magnesium concentrations varied from 2.3 to 9.1 mg L^{-1} at CAN (mean 6.3 mg L^{-1}) and from 2.7 to 10.1 mg L^{-1} at LAR (mean 7.2 mg L^{-1}). At LAR, Ca^{2+} concentrations ranged from 50.4 to 65.9 mg L^{-1} (mean 59.3 mg L^{-1}), while at CAN they span 59.7–84.9 mg L^{-1} with an average of 67.6 mg L^{-1}. As a result, total hardness, mostly controlled by Ca^{2+} and Mg^{2+}, is slightly higher at CAN (average 19.3 °fH) than at LAR (average 17.7 °fH). Sodium concentrations are low at both springs, ranging from 1.1 to 3.1 mg L^{-1} at LAR (mean: 1.8 mg L^{-1}) and from 1.0 to 5.1 mg L^{-1} at CAN (mean: 2.4 mg L^{-1}). Potassium concentrations are similarly low, with values between 0.2 and 0.74 mg L^{-1} (mean: 0.43 mg L^{-1}) at LAR and between 0.28 and 0.90 mg L^{-1} (mean: 0.42 mg L^{-1}) at CAN. Among the major anions, bicarbonate ranges from 151 to 223 mg L^{-1} at LAR (mean: 183 mg L^{-1}) and from 162 to 248 mg L^{-1} at CAN (mean: 200 mg L^{-1}). Chloride and fluoride display limited variability and similar concentrations at both sites. Sulphate concentrations are generally low at LAR (4.1–10.7 mg L^{-1}) but more variable at CAN (6.0–37.4 mg L^{-1}), with the highest value recorded in a single sample in October 2020.

The two springs show comparable pH values (mean: 7.73 at CAN and 7.75 at LAR), although CAN exhibits a wider range (7.5–8.26) compared to LAR (7.58–7.94). Alkalinity is slightly higher at CAN (mean: 169 mg L^{-1} as $CaCO_3$) than at LAR (159 mg L^{-1} as $CaCO_3$), consistent with the higher calcium concentrations observed at this spring. Piper diagrams (Fig. S12) indicate that both springs belong to a calcium–bicarbonate hydrochemical facies, confirming that groundwater feeding the springs circulates mainly within carbonate lithologies. The clustering of samples in the Ca-HCO sector and their limited temporal dispersion suggest a relatively stable geochemical signature over the monitoring period, despite seasonal hydrological variability.

3.3. Isotopic composition of precipitation

Additional samples for isotopic analysis were collected in November 2019 and June 2021, resulting in higher data density during these periods compared to the chemical dataset. Table S2 and Fig. S13 summarize the results of isotopic analyses of precipitation collected at the CLR and VIT stations. At the CLR rain gauge, $\delta^{18}O$ values range from −14.14‰ (January 2021) to −2.74‰ (June 2019) with an average of −8.31‰, while δ^2H values vary between −104.13‰ (January 2021) and −15.98‰ (June 2019), average −54.01‰. Deuterium excess (d; average: 12.47‰) spans from 5.90‰ to 18.02‰, measured in June 2019 and November 2019, respectively. At the VIT station, $\delta^{18}O$ values (average: −6.30‰) range from −9.05‰ (January 2021) to −0.04‰ (June 2019), and δ^2H values (average: −41.25‰) from −64.67‰ (November 2020) to −0.80‰ (June 2019). Deuterium excess values show a wider variability, with a minimum of −0.50‰ in June 2019 and a maximum of 23.62‰ in November 2019 (average: 9.12‰). These values are consistent with previously published data for the study area and, more broadly, for northeastern Italy (Longinelli and Selmo, 2003; Giustini et al., 2016; Masiol et al., 2021). Precipitation collected in Cansiglio (1033 m a.s.l., approx. 1 km from CLR) during 2007–2010 (Masiol et al., 2021), recorded mean values of −8.79‰ (range: −15.34‰ to −4.20‰) for $\delta^{18}O$, −58.32‰ (range: −118.3‰ to −23.9‰) for δ^2H, and 12.01‰ (range: 4.39‰ to 16.98‰) for d-excess. The data highlights a pronounced seasonal variability, with less negative delta values in June–July and more negative values in December–February (Fig. S14). Lower delta values, generally observed during colder periods and at the higher-altitude site (CLR), reflect the well-established positive relationship between the isotopic composition of precipitation and air temperature, which is particularly evident at mid to high latitudes.

The $\delta^{18}O$ and δ^2H values measured in precipitation collected at CLR and VIT were used to define the Local Meteoric Water Line (LMWL). Fig. S15 presents both the overall LMWL and its seasonal subdivision, derived from a continuous two-year dataset spanning September 2019 to August 2021. The isotopic composition of precipitation observed in this study resulted in a slope of 7.8 (95% confidence intervals (c.i.) computed by equi-tailed two-sided nonparametric confidence intervals over 1000 repetitions: 4.91–11.13) and an intercept of 7.53 (c.i. 7.11–7.94), which in agreement with values reported in the literature for northern Italy (slope = 8.04, intercept = 11.47; Giustini et al. 2016) and for NE Italy (slope = 7.8, intercept = 8.87; Masiol et al., 2021), indicating comparable moisture sources and atmospheric processes and supporting the regional representativeness of the isotopic dataset.

3.4. Isotopic composition of springs

The isotopic values of the two springs show very limited temporal variability, with mean values falling between the average isotopic compositions of precipitation collected at CLR and VIT. At LAR, $\delta^{18}O$ values range from −8.19‰ to −7.42‰ (average: −7.65‰), while δ^2H values vary between −54.19‰ and −46.98‰ (average: −49.07‰), both extremes recorded in May 2021 and September 2020, respectively (Table S2 and Fig. S13). Deuterium excess spans from 10.47‰ to 13.06‰ (average: 12.10‰).

At CAN, $\delta^{18}O$ values range from −7.89‰ to −6.70‰ (average: −7.48‰), and δ^2H values from −52.24‰ to −42.85‰ (average: −48.03‰) (Table S2 and Fig. S13). Deuterium excess values varied between 10.43‰ to 12.92‰. Fig. 4 shows the $\delta^{18}O$ and δ^2H relationships for all the rain samples and the springs separately (not only 2-year dataset, as previously reported for LMWL of precipitation data). The regression lines are well aligned, indicating negligible secondary evaporation in waters discharging at the springs. The angular coefficient and

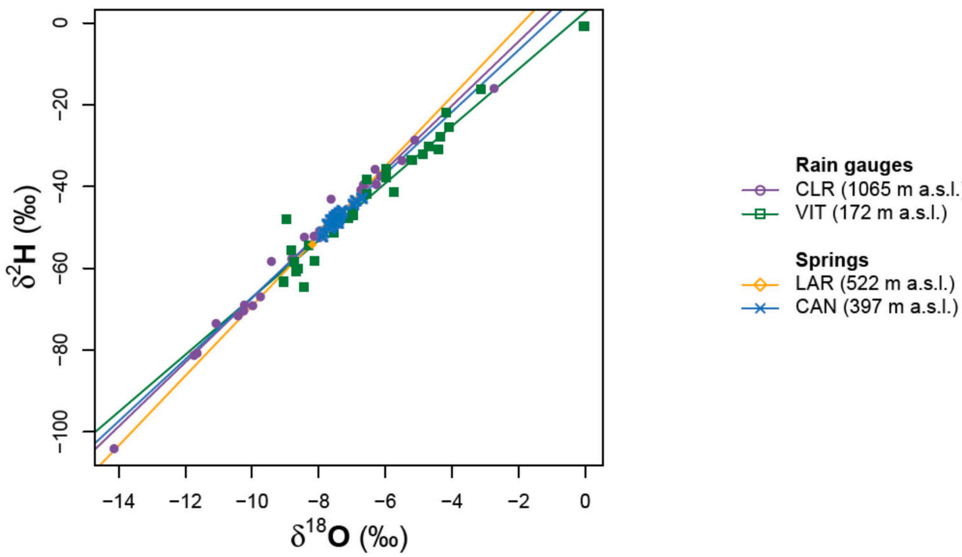

Fig. 4. $\delta^{18}O$ – $\delta^{2}H$ relationships obtained using separately the isotopic values of the rain gauges and springs (all data used);the slope – intercept coefficient relationships and their 95th confidence intervals (all data used) are shown in Fig. S16.

intercept of the different lines are also compared along with their confidence intervals (Fig. S16). Results show that CAN is more closely aligned with CLR precipitation than with VIT, while the LAR spring aligns exclusively with CLR. This suggests that recharge to both springs is predominantly controlled by precipitation conditions representative of the CLR area.

Fig. 5 shows the temporal evolution of $\delta^{18}O$, $\delta^{2}H$, and d-excess measured in spring waters and precipitation. In contrast to the clear seasonal variability observed in precipitation, which is controlled by both seasonal and altitudinal effects, the isotopic composition of the springs remains remarkably stable over time. This limited variability suggests efficient mixing of recharge waters within the aquifer and a significant buffering effect associated with groundwater storage and residence time, which dampens short-term isotopic signals from individual precipitation events. Despite this overall stability, some differences between the two springs are evident. Several samples (notably November 2019, May 2020, and August 2021) show more depleted $\delta^{18}O$ and $\delta^{2}H$ values at LAR compared to CAN, likely reflecting the higher elevation of the LAR recharge area. A pronounced isotopic depletion observed in both springs during May–June 2021 is plausibly linked to the melting of a substantial winter snowpack (approximately 50 cm), indicating episodic transmission of seasonally distinctive recharge signals through the aquifer.

Filippini et al. (2018) reported $\delta^{18}O$ values ranging from approximately −9.9‰ to −8.5‰ and $\delta^{2}H$ values from approximately −64‰ to −54‰ for the three major basal springs (Santissima, Molinetto, and Gorgazzo; Fig. 1b) of the Cansiglio-Monte Cavallo karst aquifer system during 2015 (Santissima exhibited the more negative values). These values are consistently more depleted than those measured at the LAR and CAN springs. Given that no significant long-term trends in the

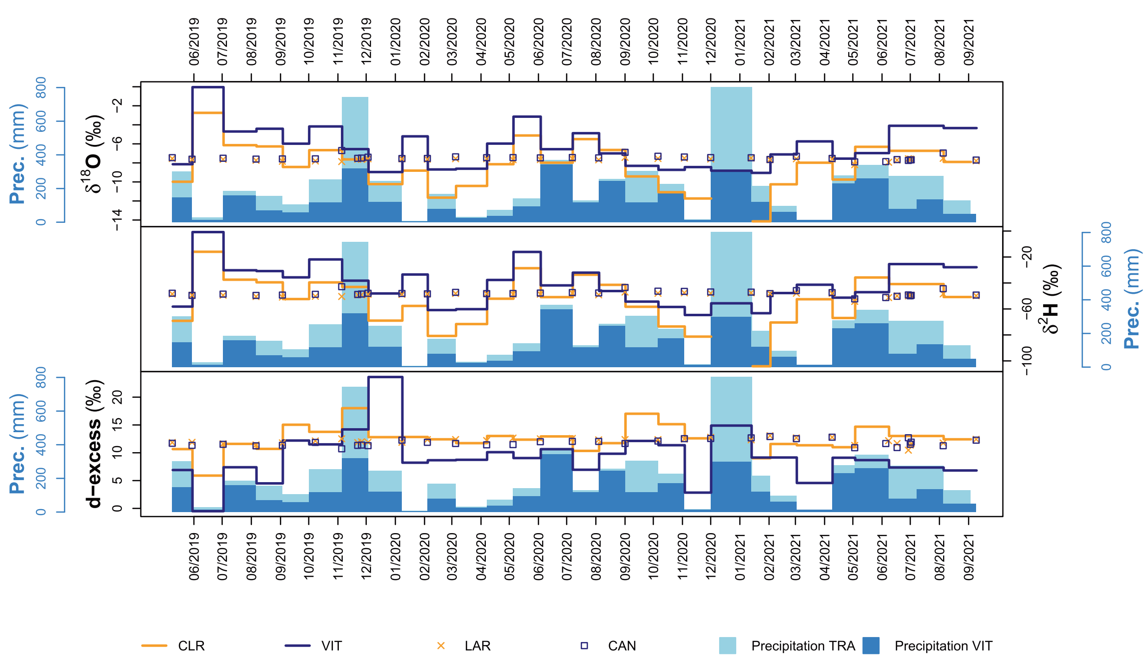

Fig. 5. Temporal variation of $\delta^{18}O$, $\delta^{2}H$, and d-excess measured at the two springs (LAR and CAN) and at the two rain gauges (CLR and VIT) along with period-cumulated precipitation amount measured at the two AWSs (TRA and VIT).

isotopic composition of precipitation have been detected in the area (Masiol et al., 2021), this difference is explained by a higher mean recharge elevation for the three major springs. Consequently, the isotopic evidence suggests that LAR and CAN are not directly connected to the main regional karst flow system. Nevertheless, a partial hydraulic connection through overflow from higher carbonate domains or fault-controlled pathways cannot be excluded based on the available data.

3.5. Spring vulnerability

The VESPA index was calculated using hourly data collected by CTD probes over the entire monitoring period for both springs (Table 1); its uncertainty was also quantified by propagating measurement uncertainties (temperature, EC) and prediction + measurement uncertainty (discharge). Although continuous measurements for a complete hydrological year were not available due to data gaps, the proportion of missing data at LAR did not exceed 10% and did not persist for more than two consecutive months. This supports the reliability of the results and is consistent with Banzato et al. (2017), who reported that up to 10–20% missing data are acceptable, if gaps do not extend beyond 2–3 consecutive months. At CAN spring, a higher proportion of missing data was recorded, particularly for discharge, as values below ~3 L s^{-1} were excluded due to hydraulic management operations. Nevertheless, missing data for temperature and EC remained below 10%, whereas discharge exhibited approximately 35% missing data, with the longest continuous gap lasting about three months. Since data gaps may introduce a systematic bias into the statistics used to estimate the three factors (β, γ, ρ) and, consequently, the vulnerability index, the robustness of these estimates was further assessed under different gap-filling scenarios (still including prediction and measurement uncertainties; Table 1). Specifically, the calculations were repeated 1000 times using randomly selected subsets containing 80% (4/5) of the original observations. This resampling procedure simulates the effect of a further 20% reduction in data availability, corresponding to the maximum threshold recommended by Banzato et al. (2017) while keeping the total datasets longer than 19 months. The resulting distributions of the estimated parameters were then used to derive uncertainty ranges for the three factors as well as for the V index.

LAR yielded V in the 0.36–0.77 range (medium vulnerability; $0.1 < V < 1$), whereas CAN 22.9–45.7 (very high vulnerability; $V > 10$). The coefficient ρ was used to identify the dominant hydrodynamic behaviour as classified by Galleani et al. (2011) (Section S2), suggesting that groundwater flow is predominantly controlled by replacement processes ($\rho = -0.33$ [−0.4 to −0.26] at LAR and −0.59 [−0.71 to −0.49] at CAN). This classification is consistent with the discharge-temperature-EC behaviour previously described for LAR; however, at CAN, which also has a high value of vulnerability V, it contrasts with event-scale discharge-temperature-EC observations that might suggest a piston-flow component (Fig. S8).

This apparent contradiction arises because the two analyses characterize groundwater dynamics at different temporal scales and therefore provide complementary information. The event-scale chemograph captures the short-term response of the spring to individual recharge events, whereas the VESPA index, and particularly ρ, is computed over the entire monitoring period and provides an integrated description of the dominant hydrogeological behaviour at multi-seasonal timescales (more than 19 months of observations for CAN). In this study, the complementarity between the event-scale chemograph response and the annual-scale VESPA classification becomes clearer when the associated uncertainties are considered. Although the correlation coefficient classifies the springs as predominantly replacement-dominated on an annual basis, the corresponding correlation factors, c (ρ), fall within the range 0.26–0.4 and 0.49–0.71 for LAR and CAN, respectively (Table 1), which slightly overlap the interval associated with piston-flow behaviour (Type B) reported by Galleani et al. (2011). Although not conclusive, this overlap is consistent with the event-scale observations and supports the interpretation of a mixed hydrodynamic response rather than a single flow mechanism.

The vulnerability class derived with the MDHT approach (Civita, 2008) was estimated from daily-mean discharge data by selecting three recession events (one per monitoring year) in which discharge decreased monotonically, i.e., without superimposed recharge pulses (hence, these events did not necessarily coincide with the annual maximum discharge peaks). MDHT values at LAR (15–21 days; 9–22 days also accounting for the discharge uncertainty) classify the spring under the high and medium vulnerability, whereas CAN exhibits consistently short MDHT values (2–3 days; 1–4 days also accounting for the discharge uncertainty), corresponding to very high vulnerability. Taken together, both methods indicate higher vulnerability and faster hydrological response at CAN relative to LAR, while LAR displays a more attenuated response consistent with longer circulation pathways.

Table 1
Results of the calculation of VESPA index for the two springs. Details of the method are reported in SectionS2 (β = temperature variability factor; γ = discharge factor; ρ = correlation coefficient between discharge and electrical conductivity calculated over a one-year period; V = VESPA index). LAR and CAN are computed over the entire dataset, while CAN* reports the minimum and maximum values of the factors and V assessed under different gap-filling scenarios.

	β	γ	ρ	V
LAR	0.51	3.37	−0.33	0.56
	[0.36;0.65]	[3.07;3.73]	[−0.4;−0.26]	[0.36;0.77]
CAN	9.11	6.51	−0.59	35.2
	[6.53;11.68]	[5.75;6.92]	[−0.68;−0.51]	[22.9;45.7]
CAN*	[4.08;11.68]	[5.57;7.19]	[−0.71;−0.49]	[14;38.7]

3.6. Catchment areas and average recharge elevations

The potential recharge area was delineated using a multi-evidence approach that combined a Digital Elevation Model (DEM) with local geological mapping and targeted field observations of the texture and structure of rock and soil outcrops upstream of the springs. The potential recharge zone is therefore inferred to extend from the summit area of Mt. Pizzoc downslope toward the spring locations (Fig. 1c-d; Fig. S17), following the main topographic gradients and structurally controlled pathways. For LAR, the strictly topographic catchment area is limited to 0.016 km^2 along a portion of the hogback, whereas the potential recharge area extends to ~1.18 km^2. For CAN, a further 0.31 km^2 is estimated downslope to the LAR area, resulting in a total area of 1.49 km^2 (Fig. S17).

From a lithostratigraphic perspective, the area includes several formations characterized by composition and textural properties, which can be broadly grouped into three main categories (Fig. 1d): (i) layered cherty limestones, (ii) massive limestones, and (iii) marls-clays-sandstone-conglomerates. The area, hypothetically interpreted as the recharge watershed of the springs, is characterized by two main lithological groups and by unconsolidated debris. At the higher elevation, on the upper slope, crop out marly limestone (Scaglia Rossa) and reef-slope grainstone (Calcare di Fadalto). In the lower part of the mountain flank, at the footwall of the high angle-fault (Fig. 1d), several steeply tilted formations are exposed, ranging from deep sea sediments to the synorogenic molassic units, including glauconitic sandstone, bioclastic sandstone, thick marl and clay layers, and subordinate conglomerate outcrops. Morphologically, the slope has a fairly uniform gradient and is largely covered by locally cemented talus debris, while at the lower elevation hogback hills runs parallel to the mountain flank.

From a hydrogeological perspective, the molassic sequence behaves predominantly as an aquiclude, except for a few more permeable layers, whereas the reef grainstone constitutes a karst aquifer. These two groups are separated by a probably high-angle fault dipping eastward. The talus cover consists mainly of gravel-sized clasts derived from the cliffs by gravitational processes or redeposited by debris-flow events; locally, the debris is cemented and contains large voids between the clasts (high porosity).

In addition to orography and lithology, spatial precipitation gradients further constrain effective recharge areas. Thus, rainfall and discharge data can therefore be used to further refine the delineation of recharge zones (e.g., Custodio and Jodar, 2016) and to better constrain hydrogeological connections with discharging springs, particularly in mountainous carbonate settings where recharge is predominantly diffuse. Higher precipitation at the upper AWS (+69% in TRA with respect to VIT) is expected to enhance recharge in high-elevation sectors where infiltration conditions are favourable. In addition, the Montaner fault line (~900 m a.s.l.; Fig. 1d) may increase fracturing within flysch units and promote hydraulic connectivity with circulating waters in or from platform carbonates.

A simple quantitative closure supports the interpretation that the LAR spring cannot be sustained by its strictly topographic catchment alone. Therefore, the extent of the recharge area for LAR was estimated using simplified hydrological budgets (Kreye et al., 1996). The mean discharge (~8.9 L s^{-1}) corresponds to an annual volume of approximately $2.8 \cdot 10^5$ m^3 y^{-1}. Assuming a representative annual precipitation of 2600 mm y^{-1} and, as a first-order limiting case, negligible evapotranspiration, runoff, and interannual storage change, the minimum area required to sustain this discharge is ~0.11 km^2. This value falls within the range estimated from the annual water-balance calculations (0.08–0.12 km^2). By contrast, the strictly topographic catchment of LAR (~0.016 km^2) would provide ~1.3 L s^{-1} under the same precipitation assumption and is therefore far too small to explain the observed discharge. Specifically, precipitation measured at TRA was further compared with spring discharge over the entire monitoring period or distinct hydrologic years (Table S3). Incomplete discharge records restrict the analysis to two complete annual periods, indicating a possible recharge area ranging from 0.08 km^2 (October 2019 to September 2020) to 0.124 km^2 (October 2020 to September 2021), compared with a strictly topographic catchment of only about 0.016 km^2 (Fig. S17). These values should be considered minimum estimates of the recharge area, as they assume null runoff and null evapotranspiration (Kreye et al., 1996). When net precipitation is recalculated by accounting for potential evapotranspiration losses (estimated using the method by Hargreaves, 1994) while still assuming negligible runoff, the inferred (net) recharge area increases to 0.110 to 0.169 km^2 (Table S3). Although larger than the strictly topographic catchment, this area remains approximately one order of magnitude smaller than the overall potential catchment area (Fig. 1c,d). This discrepancy indicates that LAR receives recharge from areas extending beyond the local surface watershed, through laterally redistributed flow paths controlled by slope deposits, lithological contrasts, and structural discontinuities. Thus, the water-balance estimate does not contradict the conceptual model but rather supports the need to distinguish between the small topographic catchment, the minimum effective recharge area, and the broader potential hydrogeological contributing area.

The isotopic composition of water in precipitation can further refine the estimation of recharge areas, as it is strongly influenced by elevation through the so-called altitude effect. This temperature-dependent process results from the combined action of (i) enhanced equilibrium fractionation associated with adiabatic cooling during air-mass uplift and (ii) progressive depletion of heavy isotopes driven by Rayleigh distillation as condensation proceeds under decreasing temperatures (e.g., Gat, 2010). Based on the complete dataset, the unweighted average vertical isotopic gradients calculated between the CLR and VIT stations for all single monthly records are −0.23‰ δ^{18}O‰/100 m (range: −0.57 to 0.07‰/100 m) and −1.5‰ δ^2H‰/100 m (range: −4.6 to 1.3‰/100 m). Steeper gradients are generally observed in winter (−0.36‰ δ^{18}O ‰/100 m; −2.9‰ δ^2H‰/100 m), while shallower gradients occur in summer (−0.19‰ δ^{18}O‰/100 m; −1‰ δ^2H‰/100 m). However, amount-weighted average vertical isotopic gradients are possible only in the August 2019-July 2020 period due to data gap (Dec 2020) with a slightly lower value: −0.19‰ $\delta^{18}O_p$‰/100 m; −1.3‰ δ^2H_p‰/100 m. These values are fully consistent with those previously reported for NE Italy (e.g., −0.19 δ^{18}O‰/100 m in Longinelli and Selmo (2003); −0.22 δ^{18}O‰/100 in Giustini et al. (2016), and −0.17 $\delta^{18}O_p$‰/100 m in Masiol et al. (2021)). The close agreement with regional gradients supports the representativeness of the dataset and confirms that elevation exerts a primary control on the isotopic signature of precipitation in the study area, providing a robust framework for interpreting recharge elevations and groundwater flow paths feeding the investigated springs.

Recharge elevations were therefore estimated using the isotopic altitude gradient derived from amount-weighted mean δ^{18}O values of precipitation and the mean isotopic composition of spring waters over one hydrological year (August 2019-July 2020; only the first hydrological year is used because the second year has a data gap in Dec 2020). The procedure also accounted for the analytical precision of the isotopic measurements for both precipitation and spring water, uncertainty in precipitation amount collected with rain gauges, and the variability of spring-water isotopic values over the hydrological year to estimate 95% confidence intervals by nonparametric bootstrap (1000 replicates with replacement). Applying the altitude-δ^{18}O relationship to annual mean spring-water δ^{18}O yielded mean recharge elevations of 822 m a.s.l. [c.i. range 732–879] for LAR and 700 m a.s.l. [c.i. range 617–767] for CAN (Fig. S17a;b). Clipping the overall recharge area by these elevation ranges and the lateral extension of the catchment areas yielded surfaces of 0.2 and 0.3 km^2 for LAR and CAN, respectively. The distributions of the estimated mean recharge elevations of the springs are statistically different, as indicated by a nonparametric Mann-Whitney U test ($p < 0.05$). Discharge-weighted spring δ^{18}O estimates produced consistent results within the c.i. boundaries (803 and 714 m a.s.l., respectively).

The same calculations were repeated using the individual isotopic measurements from the two springs in order to assess the temporal variability of recharge-area estimates while keeping the annual altitude-δ^{18}O relationship. The results (Fig. S18) indicate that the potential recharge areas for LAR were located at higher elevations in September–November 2019 than during the rest of the hydrological year. CAN shows a similar seasonal pattern, although an anomalous value was recorded in early November 2019, indicating a recharge area at very low elevation, within the spring elevation range when the associated uncertainty is considered. In any case, this value has limited influence on the annual recharge-area estimate, and its interpretation remains unclear.

These elevation ranges largely fall within debris-covered slope sectors upslope of the springs Fig. S17). Under this view, contributions from the upper carbonate plateau (e.g., Calcare di Fadalto above 1000 m a.s.l.) remain plausible as overflow above the Montaner fault zone. Given its position into the inferred mean recharge zone for LAR, it is likely that the Montaner fault forms an aquiclude barrier, although it can be hypothesized that aquifer water may overflow into the debris and the more permeable layers into the molassic sequence. This interpretation, which considerably narrows the recharge area of LAR, is also supported by the previous simplified hydrological budget estimation (Table S3), which for LAR identifies a recharge area of only 0.08–0.124 km^2 (minimum) or 0.110–0.169 km^2 (net).

Results provide no evidence that the two springs are directly hydraulically connected to the regional Cansiglio karst system and suggest that, if such a connection exists, its contribution is likely negligible compared with that of local groundwater flow systems. This interpretation is consistent with a simple water-balance analysis for the Cansiglio Plateau based on the data of Filippini et al. (2018). Assuming negligible surface runoff and evapotranspiration, sustaining the average discharge (7.7 m^3 s^{-1}) of the two main Livenza springs draining the plateau (S1 and S2; Fig. 1b) would require a minimum recharge area of approximately 136 km^2, far exceeding the ~53 km^2 extent of the Cansiglio Plateau *sensu stricto*. This indicates that the regional karst aquifer is recharged by a substantially larger area than the plateau alone, making it unlikely that the relatively small, locally recharged LAR and CAN springs belong to the same regional groundwater flow system.

Overall, the combined isotope, hydrogeochemical, and vulnerability evidence suggests contrasting flow systems feeding the two springs. The isotope-derived mean recharge elevations place CAN at a lower effective recharge altitude than LAR, consistent with a recharge domain more focused on nearby slope sectors and a comparatively shallow circulation pattern, whereas LAR integrates recharge from higher elevations and/or longer pathways. This conceptual separation is further supported by response indicators: CAN shows markedly faster system dynamics (e.g., high VESPA and short MDHT, shorter lags between precipitation events and discharge peaks), compatible with rapid infiltration and short residence times, while LAR exhibits a more attenuated response consistent with deeper and longer circulation pathways.

The VESPA index generally supports this interpretation, although its diagnostic value should be considered with caution. At CAN, the negative correlation coefficient ($-1 \leq \rho \leq -0.2$) between discharge and electrical conductivity (Table 1) is indicative of a replacement-dominated (Type A; Galleani et al., 2011) response. However, the distinct, short-lived simultaneous increase in EC and water temperature observed at the onset of several recharge events (Fig. S8) suggests that the initial response includes a piston-flow component, whereby resident groundwater is displaced by newly infiltrating recharge water. This apparent discrepancy likely reflects the coexistence of multiple flow mechanisms during storm events and highlights a limitation of the VESPA index, which is based solely on the discharge-EC relationship and does not account for the concurrent evolution of water temperature or other hydrochemical tracers. This limitation may be particularly relevant in shallow aquifers mantled by glacial till and slope debris, where temporary storage and delayed release of infiltrating water can generate more complex chemograph responses than those typically observed in well-developed karst systems.

From a hydrogeochemical point of view, both springs fall within a Ca-HCO_3 facies, confirming dominant circulation in carbonate-rich rocks. However, the stronger and more stable carbonate signature (higher Ca^{2+} concentrations and hardness) observed at CAN is consistent with relatively direct recharge through debris-covered slope deposits rather than through fractured or karstified carbonate pathways. Under this view, the unconsolidated material likely provides a large reactive surface area, while humic acids produced by organic matter decomposition may lower pH and thereby enhance calcium carbonate dissolution. In contrast, the relatively greater variability observed at LAR is coherent with a more heterogeneous recharge setting and structurally guided flow paths that may intersect alternating carbonate and marly/flysch intervals, promoting mixing and longer water–rock interaction. Overall, these lines of evidence support a dual recharge regime in the massif, combining rapid preferential infiltration in permeable carbonate domains with slower, laterally redistributed flow where fine-grained units restrict vertical percolation.

3.7. Delineation of the protection and respect zones

Several measures can be adopted to preserve mountain springs (e.g., Viviroli et al., 2011; Papadaki, 2021), including protecting spring-side vegetation, regulating land-use practices to prevent pollution and soil degradation, and implementing sustainable water management to avoid overexploitation. In Veneto, regional legislation (DGR 1621/2019 of the Veneto Region) recommends defining a safeguard zone for springs by applying one of the established methods for assessing spring vulnerability, such as the VESPA index, with protection areas scaled to the degree of vulnerability.

In this study, the derived vulnerability levels allow for the delineation of the legally prescribed absolute protection zone (immediately surrounding the intake, with land use restricted to intake facilities and essential service infrastructure, in Italian ZTA, "*zona di tutela assoluta*") and the respect zone (a wider buffer subject to land-use restrictions aimed at preserving water quality and quantity, in Italian ZTR, "*zona di rispetto*"). There is however a discrepancy between the regulation and the scientific methods approved by the regulation itself for delineating ZTAs. According to the regulatory criterion, the ZTA is defined as a circular area with a radius of 10 m around the intake point. By contrast, the scientific methods approved within the same regulatory framework define the ZTA as a rectangular area extending at least 10 m upstream of the intake point, with lateral extensions on each side equal to three-quarters of the upstream distance. Downstream, the extension varies according to the vulnerability class: 10 m for elevated vulnerability, 5 m for high to medium vulnerability, and 2 m for low vulnerability.

Given this discrepancy, and considering the hydrogeological rationale, this study adopts the approved scientific methods for ZTA delineation, while the regulatory criterion is applied preferentially at the decision-making stage where required. This way, for LAR (moderately vulnerable) the absolute protection zone extends 20 m upstream (exceeding the minimum proposed upstream distance by a factor of two), 5 m downstream, and 15 m laterally, whereas for CAN (very high vulnerability) the absolute protection zone widens to 40 m upstream (exceeding by a factor of four), 10 m downstream, and 30 m laterally (Fig. S19).

LAR requires a ZTR extending 400 m upstream expanding with a 30° angle on both sides, these dimensions create a polygon of $\sim$0.081 km^2 that is similar to the minimum recharge area calculated by the water budget (Fig. S19). CAN instead requires that the ZTR must encompass the entire spring drainage basin. Within this regulatory framework, the safeguard zones coincide with the recharge area only for CAN, because the high-vulnerability class triggers a basin-wide respect zone, while for LAR the delineation based on regional regulations does not necessarily capture the full recharge area. This points out that vulnerability indices provide a theoretical protection requirement, but that spatial allocation must be grounded in a recharge-area hypothesis derived from hydrological and hydrogeological evidence. This coupling becomes especially important for springs sustained by intermediate circuits, where outlet-based indices alone may be insufficient to define adequate protection areas (Javadi et al., 2019). The same logic might apply to longer-circuit systems such as LAR, where contributing areas might extend well beyond the outlet surroundings. Thus, delineation should be supported by integrated reconstruction of recharge through geomorphological/cartographic analysis and geo-hydrogeological mapping, complemented where appropriate by environmental tracers, for example combining water isotope-based recharge-elevation constraints with hydrogeochemical characterization to refine recharge sources, flow paths, and contributing areas.

In this perspective, it is important to emphasize that the delineation of protection areas requires an appropriate balance among monitoring efforts, the integration of existing knowledge, and more detailed hydrogeological and geochemical/isotopic investigations. Moreover, whenever there is uncertainty about the robustness of the method used to define the extent of the recharge area, any planned land-use intervention upslope of the spring, including outside the protection zones, should be preceded by a more targeted and intensive monitoring and investigation program aimed at better constraining the recharge area, rather than simply providing baseline environmental monitoring.

Finally, a decision-support flowchart is proposed to guide the selection of the most appropriate approach for delineating spring protection zones in comparable hydrogeological settings (Fig. 6). Rather than relying solely on vulnerability-based methods, the framework uses the spring outlet setting together with local geological and hydrological conditions as the primary criteria for selecting defensible protection strategies. In this way, it supports both effective spring management and long-term groundwater quality protection. The workflow first distinguishes between springs issuing from debris deposits and springs directly connected to bedrock aquifers. For debris-controlled systems, the first step is to assess whether the upstream debris body alone can store enough water to sustain the observed discharge. If the debris cover

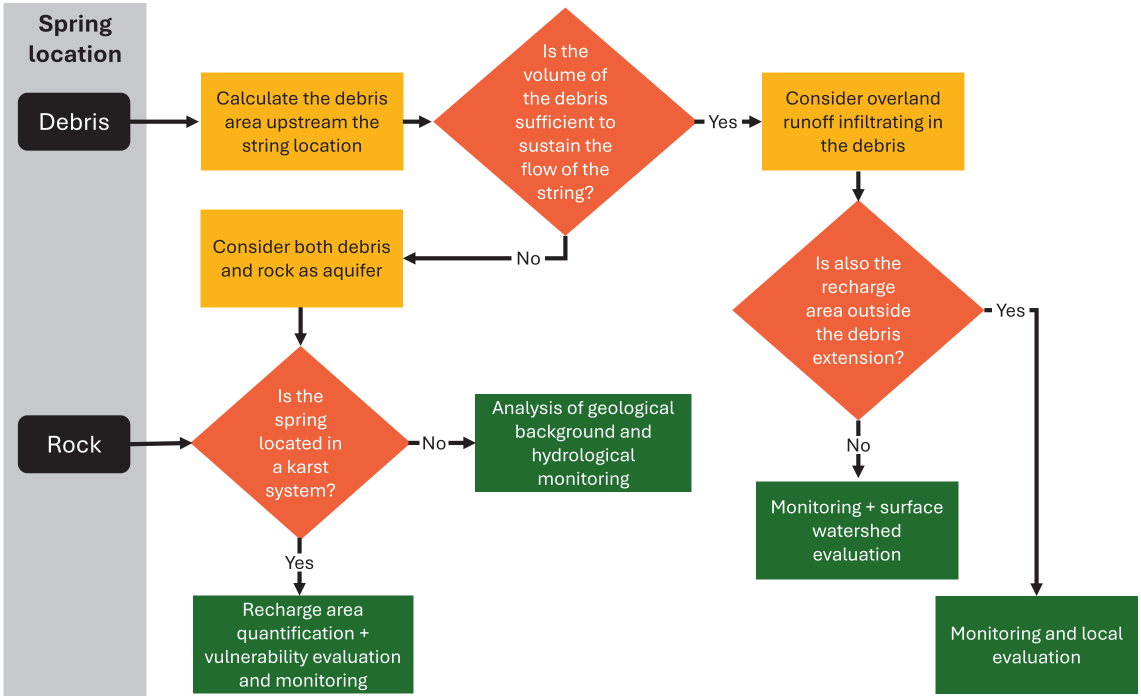

Fig. 6. Decision-support flowchart for selecting the most appropriate approach to delineate spring protection zones in different hydrogeological settings.

is sufficient, a precautionary approach based on hydro-parameter monitoring and local surface assessment is recommended; this assessment may be extended to the watershed scale where allochthonous runoff could contribute to recharge. If debris storage is insufficient, the spring is assumed to also receive input from dispersive river segments, or the underlying bedrock. In such cases, as well as for springs emerging directly from rock, the framework then evaluates the likelihood of a karst connection. Where karst conditions are likely, recharge-area quantification is combined with vulnerability assessment and monitoring. In non-karst settings, protection-zone delineation relies mainly on geological characterization and hydrological monitoring. In the case of LAR and CAN, both types of spring outlets are present, with groundwater emerging directly from the bedrock and from the overlying debris deposits. In addition, the topographic watershed alone is too small to account for the observed spring discharge, making it necessary to extend the recharge area to the debris-covered upper slopes. These findings highlight the need to redefine the protection zones by considering not only vulnerability classes but also hydrogeological and isotopic evidence. A step-by-step application of the flowchart to LAR and CAN is provided in Section S5. Overall, the flowchart provides a practical and transferable conceptual tool for selecting suitable methods to define defensible spring safeguard zones.

4. Conclusions

This study combined high-frequency monitoring of two springs (temperature, electrical conductivity, water level and, indirectly, discharge) collected with automatic devices with major-ion chemistry and stable water isotopes collected on monthly basis to characterize recharge areas and intrinsic vulnerability of two mountain springs (LAR and CAN) on the southern slope of the Cansiglio-Cavallo Massif. These springs are representative of many small mountain water supplies that require systematic monitoring and targeted protection, as they provide a key contribution to local distribution networks.

The hydrochemical facies of both springs is Ca-HCO_3, indicating dominant circulation in carbonate lithologies and a generally stable geochemical imprint over the monitoring period. Isotope evidence provides independent constraints on effective recharge conditions. Using an amount-weighted isotope-elevation relationship (August 2019–July 2020), mean recharge elevations were estimated at ~732–879 m a.s.l. for LAR and ~617–767 m a.s.l. for CAN, with consistent discharge-weighted estimates. Hydrodynamic indicators reveal markedly different system behaviours. CAN shows a fast response to precipitation and rapid drainage, reflected by very high vulnerability metrics (VESPA V in the 14–38.7 range) and short annual maximum discharge half-time (1–4 days), consistent with shallow circulation and short residence times. LAR exhibits a more buffered regime (VESPA V in the 0.36–0.77; half-life 9–22 days), indicating greater storage and longer circulation pathways. These contrasting responses highlight that springs hosted in the same massif can be sustained by substantially different flow systems, with implications for protection and management. These values, together with the mapped lithological heterogeneity and recession behaviours, support a conceptual model in which: (i) recharge of CAN is dominated by debris-covered slope sectors, with possible contributions from higher-elevation carbonate domains and structural pathways, while (ii) LAR is consistent with a more heterogeneous recharge setting and structurally controlled flow paths that likely traverse alternating carbonate and marly/flysch intervals, thereby enhancing mixing and prolonging water–rock interaction. More broadly, this study contributes to refining the conceptual hydrogeological model of the Cansiglio-Cavallo karst system. Results suggest that the LAR and CAN springs are fed by local groundwater flow systems rather than by the regional karst aquifer, providing new insights into the functioning of one of the major Mediterranean karst aquifers, highlighting the hydrogeological complexity of the massif and the need for protection strategies tailored to individual flow systems rather than assuming a single, regionally connected aquifer.

From a management perspective, the results show that outlet-based vulnerability indices are essential for ranking springs and identifying those that require stringent protection. However, they should be coupled with hydrological and hydrogeological analyses when translating vulnerability “classes” into spatial protection boundaries. In the present case, the legally defined protection zones overlap the recharge area only for the highly vulnerable CAN spring (where the respect zone extends to the entire catchment), whereas for LAR the same approach does not automatically encompass the inferred recharge area.

More broadly, this work shows the value of combining multiple complementary approaches, rather than relying on a single method, to define defensible spring protection strategies. On this basis, a decision-support flowchart was developed to guide the selection of the most appropriate approach for delineating spring protection zones in similar hydrogeological settings. The framework first distinguishes between springs controlled by debris deposits and those connected to bedrock aquifers, then uses debris storage capacity, possible external recharge contributions, and the likelihood of karst connections to identify the most suitable combination of monitoring, geological characterization, recharge-area quantification, and vulnerability assessment. In this sense, the flowchart translates the main findings of this study into a practical and transferable tool for spring management and long-term groundwater protection.

Also, vulnerability must also be considered pollutant-specific. Rapid transfer from the surface to the aquifer and spring is especially critical for microbiological contaminants, which may decay over time, and for preparedness in the event of accidental spills. By contrast, persistent pollutants entering the aquifer may not degrade, may be released over longer periods, and may be affected by spring hydrodynamics that remain only partly constrained.

CRediT authorship contribution statement

Mauro Masiol: Writing – review & editing, Writing – original draft, Investigation, Formal analysis, Data curation, Conceptualization, Funding acquisition. **Maria Battistel:** Writing – review & editing, Writing – original draft, Investigation. **Lucio D'Alberto:** Writing – review & editing, Investigation, Formal analysis, Data curation, Conceptualization. **Marianna D'Amico:** Writing – review & editing, Writing – original draft. **Giovanni Mario:** Writing – review & editing, Investigation, Formal analysis, Data curation. **Raffaele Marciano:** Writing – review & editing, Supervision, Conceptualization. **Giuliano Dreossi:** Writing – review & editing, Investigation, Formal analysis, Data curation. **Alessandro Pozzobon:** Writing – review & editing, Investigation, Data curation. **Barbara Stenni:** Writing – review & editing, Supervision, Conceptualization, Funding acquisition.

Declaration of competing interest

The authors declare that they have no known competing financial interests or personal relationships that could have appeared to influence the work reported in this paper.

Acknowledgments

This research has been carried out within the PNRR research activities of the consortium iNEST (Interconnected North-East Innovation Ecosystem) funded by the European Union Next-GenerationEU (Piano Nazionale di Ripresa e Resilienza (PNRR) Missione 4 Componente 2, Investimento 1.5 D.D. 1058 23/06/2022, ECS_00000043 –Spoke1, RT1B, CUP H43C22000540006). This manuscript reflects only the Authors views and opinions, neither the European Union nor the European Commission can be considered responsible for them. Also, the views and conclusions expressed in this paper may not reflect those of ARPAV. Authors also thankfully acknowledge: (i) ARPAV, Centro Meteorologico di Teolo, for weather data from AWS stations; (ii) Piave Servizi S.p.A. for providing access to the springs and helping in spring sample collection; (iii) the Diocese of Vittorio Veneto and the manager of Malga Le Rotte for allowing the installation of the rain gauges. Authors are grateful to the Section Editor and three anonymous referees for their insightful comments and constructive suggestions, which substantially improved the quality of the manuscript.

Statement: During the preparation of this work the authors used ChatGPT in order to improve English language and readability of the manuscript. After using this service, the authors reviewed and edited the content as needed and takes full responsibility for the content of the published article.

Appendix A. Supplementary material

Supplementary data to this article can be found online at https://doi.org/10.1016/j.jhydrol.2026.136159.

Data availability

Data will be made available on request.

References

Aller, L., Lehr, J.H., Petty, R., Bennett, T., 1987. DRASTIC: a standardized system to evaluate groundwater pollution potential using hydrogeologic setting. J. Geol. Soc. India 29 (1), 23–37. https://doi.org/10.17491/jgsi/1987/290112.

Amanzio, G., Suozzi, E., De Maio, M., 2015. Vulnerability of mountain springs affect by climatic change: a new method in a porous media aquifer in regione automa valle d' aosta. In: Engineering Geology for Society and Territory - Volume 5: Urban Geology, Sustainable Planning and Landscape Exploitation, pp. 1357–1361. https://doi.org/10.1007/978-3-319-09048-1_259.

Azimi, S., Massari, C., Formetta, G., Barbetta, S., Tazioli, A., Fronzi, D., Modanesi, S., Tarpanelli, A., Rigon, R., 2023. On understanding mountainous carbonate basins of the Mediterranean using parsimonious modeling solutions. Hydrol. Earth Syst. Sci. 27, 4485–4503. https://doi.org/10.5194/hess-27-4485-2023.

Banzato, C., Butera, I., Revelli, R., Vigna, B., 2017. Reliability of the VESPA index in identifying spring vulnerability level. J. Hydrol. Eng. 22 (6), 1–11. https://doi.org/10.1061/(asce)he.1943-5584.0001498.

Bondesan A., Busoni S., Preto N. (2013). Carta geologica della provincia di Treviso. Sezioni 064130 - Fregona-Mezzavilla - 064140 Coltura, scala 1:10.000 [In Italian: Geological map of the province of Treviso. Sections 064130 - Fregona-Mezzavilla - 064140 Coltura, scale 1:10,000].

Çallı, K.Ö., Chiogna, G., Bittner, D., Sivelle, V., Labat, D., Richieri, B., Çallı, S.S., Hartmann, A., 2025. Karst water resources in a changing world: review of solute transport modeling approaches. Rev. Geophys. 63 (1), e2023RG000811. https://doi.org/10.1029/2023RG000811.

Cancian, G., Ghetti, S., 1989. Stratigrafia del Bus de la Genziana (Cansiglio, Prealpi Venete). (Stratigraphy of Bus de la Genziana (Cansiglio, Venetian Prealps)). Studi Trentini Sc. Nat. Acta Geol., Trento 65, 125–140.

Cancian, G., Ghetti, S., Semenza, E. (1985). Aspetti geologici dell'Altipiano del Cansiglio. Lavori della Società Veneta di Scienze Naturali, suppl. 10, 79-90. In Italian.

Caputo, R., Poli, M.E., Zanferrari, A., 2010. Neogene-Quaternary tectonic stratigraphy of the eastern Southern Alps, NE Italy. J. Struct. Geol. 32, 1009–1027. https://doi.org/10.1016/j.jsg.2010.06.004.

Castiglioni, G.B., 1964: Forme del Carsismo superficiale dell'Altipiano del Cansiglio (Morphological features of epigean karst of the Pian Cansiglio).- Atti Istituto Veneziano di Scienze Lettere ed Arti, 122, 327-344.

Çelik, M., Çallı, S.S., Altın, S., Çallı, K.Ö., 2024. Reducing climate impacts on karst groundwater resources by constructing a cave dam. A case study from Central Taurus Karst, Türkiye. J. Hydrol. 636, 131245. https://doi.org/10.1016/j.jhydrol.2024.131245.

Civita, M.V., 2008. An improved method for delineating source protection zones for karst springs based on analysis of recession curve data. Hydrgeol. J. 16 (5), 855–869. https://doi.org/10.1007/S10040-008-0283-4.

Civita, M.,De Maio, M. (1997). SINTACS. Un sistema parametrico per la valutazione e la cartografia della vulnerabilità degli acquiferi all'inquinamento Metodologia e Automatizzazione, Pitagora Editrice, Bologna, Italy. ISBN 9788837108991 [in Italian].

Cisneros, J.B.E., Oki, T., Arnell, N.W., Benito, G., Cogley, J.G., Döll, P., Jiang, T., Mwakalila, S.S., Field, C.B., Barros, V.R. and Dokken, D.J., (2014). Freshwater resources. In: Climate Change 2014: Impacts, Adaptation, and Vulnerability. Part A: Global and Sectoral Aspects. Contribution of Working Group II to the Fifth Assessment Report of the Intergovernmental Panel on Climate Change [Field, C.B., V.R. Barros, D.J. Dokken, K.J. Mach, M.D. Mastrandrea, T.E. Bilir, M. Chatterjee, K.L. Ebi, Y.O. Estrada, R.C. Genova, B. Girma, E.S. Kissel, A.N. Levy, S. MacCracken, P.R. Mastrandrea, and L.L. White (eds.)]. Cambridge University Press, Cambridge, United Kingdom and New York, NY, USA, pp. 229-269.

Cucchi, F., Finocchiaro, F., 2017. Karst landforms in friuli venezia giulia: from alpine to coastal karst. In: Soldati, M., Marchetti, M. (Eds.), Landscapes and Landforms of Italy. World Geomorphological Landscapes. Springer, Cham. https://doi.org/10.1007/978-3-319-26194-2_12.

Custodio, E., Jodar, J., 2016. Simple solutions for steady–state diffuse recharge evaluation in sloping homogeneous unconfined aquifers by means of atmospheric tracers. J. Hydrol. 540, 287–305. https://doi.org/10.1016/j.jhydrol.2016.06.035.

Dansgaard, W., 1964. Stable isotopes in precipitation. Tellus 16, 436–468. https://doi.org/10.3402/tellusa.v16i4.8993.

Devoti, R., Zuliani, D., Braitenberg, C., Fabris, P., Grillo, B., 2015. Hydrologically induced slope deformations detected by GPS and clinometric surveys in the Cansiglio Plateau, Southern Alps. Earth Planet. Sci. Lett. 419, 134–142. https://doi.org/10.1016/j.epsl.2015.03.023.

EEA (European Environmental Agency) (2016). European Digital Elevation Model (EU-DEM), version 1.1. https://www.eea.europa.eu/en/datahub/datahubitem-view/d08852bc-7b5f-4835-a776-08362e2fbf4b.
EEA (European Environmental Agency) (2020). CORINE Land Cover 2018 (vector). https://doi.org/10.2909/71c95a07-e296-44fc-b22b-415f42acfdf0.
Epstein, S., Mayeda, T., 1953. Variation of O18 content of waters from natural sources. Geochim. Cosmochim. Acta 4, 213–224. https://doi.org/10.1016/0016-7037(53).
Filippini, M., Squarzoni, G., De Waele, J., Fiorucci, A., Vigna, B., Grillo, B., Riva, A., Rossetti, S., Zini, L., Casagrande, G., Stumpp, C., Gargini, A., 2018. Differentiated spring behavior under changing hydrological conditions in an alpine karst aquifer. J. Hydrol. 556, 572–584. https://doi.org/10.1016/J.JHYDROL.2017.11.040.
Fiorillo, F., Guadagno, F.M., 2012. Long karst spring discharge time series and droughts occurrence in Southern Italy. Environ. Earth Sci. 65, 2273–2283. https://doi.org/10.1007/s12665-011-1495-9.
Fiorillo, F., 2014. The recession of spring hydrographs, focused on karst aquifers. Water Resour. Manag. 28 (7), 1781–1805. https://doi.org/10.1007/s11269-014-0597-z.
Fiorillo, F., Pagnozzi, M., 2015. Recharge processes of karst massifs: examples from southern Italy. In: Andreo, B., Carrasco, F., Durán, J., Jiménez, P., LaMoreaux, J. (Eds.), Hydrogeological and Environmental Investigations in Karst Systems. Environmental Earth Sciences. Springer, Berlin, Heidelberg. https://doi.org/10.1007/978-3-642-17435-3_12.
Fiorillo, F., Petitta, M., Preziosi, E., Rusi, S., Esposito, L., Tallini, M., 2015a. Long-term trend and fluctuations of karst spring discharge in a Mediterranean area (central-southern Italy). Environ. Earth Sci. 74, 153–172. https://doi.org/10.1007/s12665-014-3946-6.
Fiorillo, F., Pagnozzi, M., Ventafridda, G., 2015b. A model to simulate recharge processes of karst massifs. Hydrol. Process. 29 (10). https://doi.org/10.1002/hyp.10353.
Fiorillo, F., Leone, G., Pagnozzi, M., Esposito, L., 2021. Long-term trends in karst spring discharge and relation to climate factors and changes. Hydrogeol. J. 29, 347–377. https://doi.org/10.1007/s10040-020-02265-0.
Fiorillo, F., Pagnozzi, M., Addesso, R., Cafaro, S., D'Angeli, I.M., Esposito, L., Leone, G., Liso, I.S., Parise, M., 2022. Uncertainties in understanding groundwater flow and spring functioning in karst. In: Threats to Springs in a Changing World: Science and Policies for Protection, pp. 131–143. https://doi.org/10.1002/9781119818625.ch9.
Forestieri, A., Arnone, E., Blenkinsop, S., Candela, A., Fowler, H., Noto, L.V., 2018. The impact of climate change on extreme precipitation in Sicily, Italy. Hydrol. Process. 32 (3), 332–348. https://doi.org/10.1002/HYP.11421.
Foster, S.S.D., 1987. Fundamental concepts in aquifer vulnerability, pollution risk and protection strategy. In: Proc., Int. Conf. on Vulnerability of Soil and Groundwater to Pollutants. Netherlands Organization for Applied Scientific Research, Delft, Netherlands, pp. 69–86.
Foster, S., Hirata, R., Andreo, B., 2013. The aquifer pollution vulnerability concept: aid or impediment in promoting groundwater protection. Hydrgeol. J. 21 (7), 1389–1392. https://doi.org/10.1007/s10040-013-1019-7.
Galleani, L., Vigna, B., Banzato, C., Russo, S.L., 2011. Validation of a vulnerability estimator for spring protection areas: the VESPA index. J. Hydrol. 396 (3–4), 233–245. https://doi.org/10.1016/j.jhydrol.2010.11.012.
Gat, J.R., 2010. Isotope Hydrology: A Study of the Water Cycle. In: Series on Environmental Science and Management — Vol. 6. Imperial College Press, London.
Giustini, F., Brilli, M., Patera, A., 2016. Mapping oxygen stable isotopes of precipitation in Italy. J. Hydrol.: Reg. Stud. 8, 162–181. https://doi.org/10.1016/j.ejrh.2016.04.001.
Gizzi, M., Mondani, M., Taddia, G., Suozzi, E., Lo Russo, S., 2022. Aosta valley mountain springs: a preliminary analysis for understanding variations in water resource availability under climate change. Water 14 (7), 1004. https://doi.org/10.3390/w14071004.
Grillo, B. (2007). Contributo alle conoscenze idrogeologiche dell'Altopiano del Cansiglio. Atti e Memorie della C.G.E.B., S.A.G. CAI, Trieste, Italia, 41, 5–15. In Italian.
Grillo, B., Braitenberg, C., Devoti, R., Nagy, I., 2011. The study of karstic aquifers by geodetic measurements in Bus de la Genziana station-Cansiglio Plateau (northeastern Italy). Acta Carsol. 40 (1), 161–173. https://doi.org/10.3986/ac.v40i1.35.
Grillo, B., Braitenberg, C. (2016). Monitoraggio delle acque di fondo del Bus de la Genziana (Pian Cansiglio, Nord-Est Italia). Atti e Memorie della C.G.E.B., S.A.G. CAI, Trieste, Italia, 46, 3–14. In Italian.
Grillo, B., Braitenberg, C., Nagy, I., Devoti, R., Zuliani, D., Fabris, P., 2018. In: Cansiglio Karst Plateau: 10 Years of Geodetic–hydrological Observations in Seismically Active Northeast Italy. Springer International Publishing, Cham, pp. 171–187. https://doi.org/10.1007/9.
Hargreaves, G.H., 1994. Defining and using reference evapotranspiration. J. Irrig. Drain. Eng. 120 (6), 1132–1139. https://doi.org/10.1061/(ASCE)0733-9437(1994)120:6(1132).
IAEA (International Atomic Energy Agency), 2014. IAEA/GNIP precipitation sampling guide V2. 02 September 2014. Available at: http://www-naweb.iaea.org/napc/ih/documents/other/gnip_manual_v2.02_en_hq.pdf (accessed March 2020).
Javadi, S., Moghaddam, H.K., Roozbahani, R., 2019. Determining springs protection areas by combining an analytical model and vulnerability index. Catena 182, 104167. https://doi.org/10.1016/J.CATENA.2019.104167.
Kendall, C., Doctor, D.H., Young, M.B., 2014. In: Environmental Isotope Applications in Hydrologic Studies. Elsevier, pp. 273–327. https://doi.org/10.1016/B978-0-08-095975-7.00510-6.
Kreye, R., Wei, M. and Reksten, D. (1996). Defining the source area of water supply springs. Hydrology Branch, Ministry of Environment, Lands and Parks. https://a100.gov.bc.ca/pub/acat/documents/r17862/define_source_area_water_springs_1270680564172_39bfd69ecc8166b1a6240486ae5a1a460e6b5ea00db43413d0e81acb465c8e70.pdf.
Leone, G., Pagnozzi, M., Catani, V., Ventafridda, G., Esposito, L., Fiorillo, F., 2020. A hundred years of Caposele spring discharge measurements: trends and statistics for understanding water resource availability under climate change. Stoch. Environ. Res. Risk Assess 35 (2), 345–370. https://doi.org/10.1007/s00477-020-01908-8.
Liu, X., Hu, L., Sun, K., 2018. Analysis of spring flow change in the jinan city under influences of recent human activities. Proc. Int. Assoc. Hydrol. Sci. 379, 263–268. https://doi.org/10.5194/PIAHS-379-263-2018.
Lo Russo, S., Suozzi, E., Gizzi, M., Taddia, G., 2021. SOURCE: a semi-automatic tool for spring-monitoring data analysis and aquifer characterisation. Environ. Earth Sci. 80 (21), 1–13. https://doi.org/10.1007/S12665-021-10027-8.
Longinelli, A., Selmo, E., 2003. Isotopic composition of precipitation in Italy: a first overall map. J. Hydrol. 270, 75–88. https://doi.org/10.1016/S0022-1694(02)00281-0.
Lorenzi, V., Banzato, F., Barberio, M.D., Goeppert, N., Goldscheider, N., Gori, F., Lacchini, A., Manetta, M., Medici, G., Rusi, S., Petitta, M., 2024. Tracking flowpaths in a complex karst system through tracer test and hydrogeochemical monitoring: implications for groundwater protection (Gran Sasso Italy). Heliyon 10 (2). https://doi.org/10.1016/j.heliyon.2024.e24663.
Lucianetti, G., Penna, D., Mastrorillo, L., Mazza, R., 2020. The role of snowmelt on the spatio-temporal variability of spring recharge in a dolomitic mountain group, Italian Alps. Water 12 (8), 2256. https://doi.org/10.3390/W12082256.
Masiol, M., Zannoni, D., Stenni, B., Dreossi, G., Zini, L., Calligaris, C., Karlicek, D., Michelini, M., Flora, O., Cucchi, F., Treu, F., 2021. Spatial distribution and interannual trends of δ18O, δ2H, and deuterium excess in precipitation across North-Eastern Italy. J. Hydrol. 598, 125749. https://doi.org/10.1016/j.jhydrol.2020.125749.
Meinzer, O.E., 1923. The occurrence of ground water in the United States, with a discussion of principles. Geological Water-Supply Paper 489, USGS. https://doi.org/10.3133/wsp489.
Meneghel, M., Sauro, U., Baciga, M.L., Fileccia, A., Frigo, G., Toniello, V., and Zampieri, D. (1986). Sorgenti carsiche e erosione chimica nelle Prealpi Venete (Karstic springs and chemical erosion in the area of Prealpi Venete). Studi Trentini di Scienze Naturali - Acta Geologica, 62, 145-172. In Italian.
Milanović, P.T., 2025. The complexity of epikarst: definitions and observations. Carbonates Evaporites 40, 127. https://doi.org/10.1007/s13146-025-01162-5.
Notarnicola, C., 2020. Hotspots of snow cover changes in global mountain regions over 2000–2018. Remote Sens. Environ. 243, 111781. https://doi.org/10.1016/J.RSE.2020.111781.
Obolewski, K., Glińska-Lewczuk, K., Ożgo, M., Astel, A., 2016. Connectivity restoration of floodplain lakes: an assessment based on macroinvertebrate communities. Hydrobiologia 774 (1), 23–37. https://doi.org/10.1007/S10750-015-2530-8.
Padulano, R., Reder, A., Rianna, G., 2019. An ensemble approach for the analysis of extreme rainfall under climate change in Naples (Italy). Hydrol. Process. 33 (14), 2020–2036. https://doi.org/10.1002/HYP.13449.
Padulano, R., Costabile, P., Costanzo, C., Rianna, G., Del Giudice, G., Mercogliano, P., 2021. Using the present to estimate the future: a simplified approach for the quantification of climate change effects on urban flooding by scenario analysis. Hydrol. Process. 35 (12). https://doi.org/10.1002/HYP.14436.
Papadaki, C., 2021. Sustainable use of mountain water resources. Elsevier, pp. 281–292. https://doi.org/10.1016/B978-0-12-819342-6.00005-1.
Parise, M., Sammarco, M., 2015. The historical use of water resources in karst. Environ. Earth Sci. 74 (1), 143–152. https://doi.org/10.1007/s12665-014-3685-8.
Parise, M., Ravbar, N., Živanović, V., Mikszewski, A., Kresic, N., Mádl-Szőnyi, J., Kukurić, N.A., 2015. Hazards in karst and managing water resources quality. In: Stevanović, Z. (Ed.), Karst Aquifers—Characterization and Engineering. Professional Practice in Earth Sciences. Springer, Cham. https://doi.org/10.1007/978-3-319-12850-4_17.
Penna, D., Stenni, B., Šanda, M., Wrede, S., Bogaard, T.A., Michelini, M., Fischer, B.M.C., Gobbi, A., Mantese, N., Zuecco, G., Borga, M., Bonazza, M., Sobotková, M., Cejková, B., Wassenaar, L.I., 2012. Technical note: evaluation of between-sample memory effects in the analysis of 2H and 18O of water samples measured by laser spectroscopes. Hydrol. Earth Syst. Sci. 16, 3925–3933. https://doi.org/10.5194/hess-16-3925-2012.
Petitta, M., Banzato, F., Lorenzi, V., Matani, E., Sbarbati, C., 2022. Determining recharge distribution in fractured carbonate aquifers in central Italy using environmental isotopes: snowpack cover as an indicator for future availability of groundwater resources. Hydrgeol. J. 30 (5), 1619–1636. https://doi.org/10.1007/s10040-022-02501-9.
Petitta, M., Barberio, M.D., Barbieri, M., Cardello, G.L., Lorenzi, V., Manetta, M., Petrella, E., Gisonni, C., 2026. Differentiating groundwater recharge flowpaths in fault-controlled karstic aquifers (Gran Sasso range, Central Italy): structural, hydrochemical and isotopic investigations on the highway tunnel drainage. J. Hydrol.: Reg. Stud. 65, 103360. https://doi.org/10.1016/j.ejrh.2026.103360.
Pfahl, S., Sodemann, H., 2014. What controls deuterium excess in global precipitation? Clim. Past 10, 771–781. https://doi.org/10.5194/cp-10-771-2014.
Pintori, F., Serpelloni, E., Longuevergne, L., Garcia, A., Faenza, L., D'Alberto, L., Gualandi, A., Belardinelli, M.E., 2021. Mechanical response of shallow crust to groundwater storage variations: inferences from deformation and seismic observations in the Eastern Southern Alps, Italy. J. Geophys. Res.: Sol. Ea. 126 (2), e2020JB020586. https://doi.org/10.1029/2020JB020586.
Pochon, A., Tripet, J.P., Kozel, R., Meylan, B., Sinreich, M., Zwahlen, F., 2008. Groundwater protection in fractured media: a vulnerability-based approach for delineating protection zones in Switzerland. Hydrgeol. J. 16 (7), 1267–1281. https://doi.org/10.1007/S10040-008-0323-0.

Riva, A., 2000. Osservazioni geologiche sul Bus della Genziana (1000 V TV) (Geological observations about Bus della Genziana (1000 V TV)). Speleologia Veneta 8, 154–156.
Somers, L.D., McKenzie, J.M., 2020. A review of groundwater in high mountain environments. Wiley Interdiscip. Rev. Water 7 (6), 1475. https://doi.org/10.1002/wat2.1475.
Stevanović, Z., 2019. Karst waters in potable water supply: a global scale overview. Environ. Earth Sci. 78, 662. https://doi.org/10.1007/s12665-019-8670-9.
Toreti, A., Fioravanti, G., Perconti, W., Desiato, F., 2009. Annual and seasonal precipitation over Italy from 1961 to 2006. Int. J. Climatol. 29, 1976–1987. https://doi.org/10.1002/joc.1840.
Torresan, F., Fabbri, P., Piccinini, L., Dalla Libera, N., Pola, M., Zampieri, D., 2020. Defining the hydrogeological behavior of karst springs through an integrated analysis: a case study in the Berici Mountains area (Vicenza, NE Italy). Hydrgeol. J. 28 (4), 1229–1247. https://doi.org/10.1007/s10040-020-02122-0.
Vincenzi, V., Riva, A., Rossetti, S., 2011. Towards a better knowledge of Cansiglio karst system (Italy): results of the first successful groundwater tracer test. Acta Carsologica 40 (1), 147–159. https://doi.org/10.3986/AC.V40I1.34.
Viviroli, D., Dürr, H.H., Messerli, B., Meybeck, M., Weingartner, R., 2007. Mountains of the world, water towers for humanity: typology, mapping, and global significance. Water Resour. Res. 43 (7), 7447. https://doi.org/10.1029/2006WR005653.
Viviroli, D., Archer, D.R., Buytaert, W., Fowler, H.J., Greenwood, G.B., Hamlet, A.F., Huang, Y., Koboltschnig, G., Litaor, M.I., López-Moreno, J.I., Lorentz, S., 2011. Climate change and mountain water resources: overview and recommendations for research, management and policy. Hydrol. Earth Syst. Sci. 15 (2), 471–504. https://doi.org/10.5194/hess-15-471-2011.
Wu, W.Y., Lo, M.H., Wada, Y., Famiglietti, J.S., Reager, J.T., Yeh, P.J.F., Ducharne, A., Yang, Z.L., 2020. Divergent effects of climate change on future groundwater availability in key mid-latitude aquifers. Nat. Commun. 11 (1), 3710. https://doi.org/10.1038/s41467-020-17581-y.
Xanke, J., Goldscheider, N., Bakalowicz, M., Barberá, J.A., Broda, S., Chen, Z., Ghanmi, M., Günther, A., Hartmann, A., Jourde, H., Liesch, T., 2024. Carbonate rocks and karst water resources in the Mediterranean region. Hydrgeol. J. 32 (5), 1397–1418. https://doi.org/10.1007/s10040-024-02810-1.